ISSN 0869-5938, Stratigraphy and Geological Correlation, 2021, Vol. 29, No. 5, pp. 518–547. © Pleiades Publishing, Ltd., 2021.
Russian Text © The Author(s), 2021, published in Stratigrafiya, Geologicheskaya Korrelyatsiya, 2021, Vol. 29, No. 5, pp. 27–58.

Bio-, Chemo-, and Magnetostratigraphy of the Santonian–Campanian Boundary in the Kudrino and Aksu-Dere Sections (Southwestern Crimea): Problems of Global Correlation and Selection of the Lower Boundary Stratotype of the Campanian. 2. Magneto- and Chemostratigraphy, Discussion

A. Yu. Guzhikov[a, *], E. Yu. Baraboshkin[b, c], G. N. Aleksandrova[c], I. P. Ryabov[a], M. A. Ustinova[c], L. F. Kopaevich[b], G. V. Mirantsev[d], A. B. Kuznetsov[e], P. A. Fokin[b], and V. L. Kosorukov[b]

[a] *Saratov National Research State University, Saratov, 410012 Russia*
[b] *Moscow State University, Moscow, 119991 Russia*
[c] *Geological Institute, Russian Academy of Sciences, Moscow, 119017 Russia*
[d] *Borissiak Paleontological Institute, Russian Academy of Sciences, Moscow, 117997 Russia*
[e] *Institute of Precambrian Geology and Geochronology, Russian Academy of Sciences, St. Petersburg, 199034 Russia*
**e-mail: aguzhikov@yandex.ru*

Received December 11, 2020; revised March 8, 2021; accepted March 25, 2021

Abstract—The paper continues a complex study of the Santonian–Campanian boundary of the Aksu-Dere and Kudrino-2 sections (Bakhchisarai region, Southwestern Crimea), the sedimentological and biostratigraphic data on which are provided in paper 1. This work presents the paleomagnetic, rock magnetic, and geochemical data on C and O stable isotopes. The $^{87}Sr/^{86}Sr$ values of limestones increase upward the section: from 0.70741 to 0.70752 in Aksu-Dere and from 0.70750 to 0.70755 in Kudrino-2. On the basis of the results, the outcrops are correlated and the Kudrino–Aksu-Dere composite section is compilled, in which we identified paleontological, paleomagnetic, and isotopic markers necessary for the identification of the Santonian–Campanian boundary. The biostratigraphic boundaries are calibrated against the geomagnetic reversal 34n–33r and the SCBE isotopic event; thus, the base of the Campanian Stage should be determined by the base of the Chron 33r. In the volume of the geological record of the Santonian–Campanian boundary, saturation in guide fossil forms, and complex study, the composite section matches the candidates for a Global Boundary Stratotype Section and Point of the Campanian in North Texas and Southern England. This allows us to propose it as one of the candidates of the stratotype or an auxiliary section of the lower boundary of the Campanian Stage.

Keywords: Upper Cretaceous, Santonian, Campanian, magnetostratigraphy, dinocysts, benthic foraminifers, planktonic foraminifers, nannoplankton, crinoids, stable carbon isotopes, oxygen and strontium isotopes, stratotype, Crimea

DOI: 10.1134/S086959382105004X

INTRODUCTION

Paper 2 presents the results of comprehensive studies of the Santonian–Campanian boundary in the Aksu-Dere and Kudrino-2 sections (Southwestern Crimea). It includes the magnetostratigraphic and chemostratigraphic data which are necessary for the study of the reference sections along with paleontological data provided in the paper 1. The magnetostratigraphic method studies the remanent magnetization of rocks and minerals, which recorded the direction of the Earth's magnetic field in the past, as well as other magnetic properties of rocks (Molostovskii and Khramov, 1997). The isotopic chemostratigraphy is based on the long-term variations in $\delta^{13}C$, $\delta^{18}O$, and $^{87}Sr/^{86}Sr$ values of marine sediments, which are able to preserve the initial isotope characteristics (Jones et al., 1994; Kuznetsov et al., 2018; McArthur et al., 2012; Wierzbowski et al., 2017). The C and Sr isotope analysis is used for the carbonate sediments, deposited in situ in open marine basins connected to the ocean and which are less altered during epigenesis. Recently, many Late Mesozoic reference sections were charac-

terized by C and Sr isotopes, which allowed refined correlation of the carbonate rocks and their age (Kuznetsov et al., 2017; Rud'ko et al., 2014; Wagreich et al., 2010; Wolfgring et al., 2018a; Zakharov et al., 2013).

MAGNETOSTRATIGRAPHY

Rock magnetic and magnetic mineralogical studies included the measurements of the following parameters: magnetic susceptibility K and its anisotropy (AMS), magnetic susceptibility K_t after rock heating at 500°C for an hour (the increase $dK = K_t - K$ reflects the amount of finely dispersed pyrite in sample due to a phase transition of nonmagnetic FeS_2 to strongly magnetic Fe_3O_4 at >400°C), natural remanent magnetization $\mathbf{J}_n$ (NRM), remanent saturation magnetization $\mathbf{J}_{rs}$ (maximum possible remanent magnetization in a sample created by an artificial magnetic field), the field $\mathbf{B}_s$ in which $\mathbf{J}_{rs}$ is acquired, and the field $\mathbf{B}_{cr}$ corresponding to remanent coercivity which should be applied for complete destruction of $\mathbf{J}_{rs}$ of a sample. In addition to experimental characteristics, we also calculated the following parameters: factor Q (Königsberger ratio: $\mathbf{J}_n$/induced magnetization), parameter of rigidity $S = -\mathbf{J}_{r(-300)}/\mathbf{J}_{rs}$ (where $\mathbf{J}_{r(-300)}$ is the remanent magnetization after impact by field of 300 mT which is reverse to the direction of saturation field), and $K/\mathbf{J}_{rs}$ ratio. Factor $Q \geq 1$ indicates a high degree of ordering of magnetic moments of particles. The values of parameter S close to 0 and 1 indicate dominant magnetically strong and magnetically soft minerals in a sample, respectively. The $K/\mathbf{J}_{rs}$ ratio is proportional to the average size of ferromagnetic grains.

Selected samples were subjected to thermomagnetic analysis (TMA) on a TAF-2 fraction thermoanalyzer ("magnetic balance") to reveal the correlations between magnetization ($\mathbf{J}$) and temperature (T) and were studied on a J_meter coercivity spectrometer. The K values were measured on a MFK1-FB kappabridge and the $\mathbf{J}_n$ values were analyzed on a JR-6 spinmagnetometer and a 2G-Enterprices cryogenic magnetometer at the Institute of Physics of the Earth, Russian Academy of Sciences (IPE RAS, Moscow). The hysteresis characteristics ($\mathbf{J}_{rs}$, $\mathbf{B}_{cr}$) were detected using a regulated electric magnet with a maximum intensity of 700 mT (thus, in this work, $\mathbf{J}_{rs}$ is accepted as the remanent magnetization after impact of a field with intensity of 700 mT, which is sufficient for saturation of magnetically soft samples). The dK values were measured after heating of samples in a SNOL-6/11-B oven. The AMS data were analyzed in the Anisoft 5.1.03 program (agico.com).

In the rock magnetic respect, the sections include two complexes: lower rock magnetic (PC-1) in structure of the Member XV and the Submember XVIa and upper (PC-2) in structure of Submembers XVIb–XVId and the Member XVII. The lower complex is characterized by a minimum magnetic susceptibility ($<1 \times 10^{-5}$ SI units excluding the Submember XVa and the lower parts of the Submember XVb, where K value reaches $1.5–1.7 \times 10^{-5}$ SI units) and relatively high natural remanent magnetization (the $\mathbf{J}_n$ values vary from 0.1 to 0.8×10^{-3} A/m, regularly decreasing up the section) and high factor Q (mostly, 1–5). In contrast, the upper complex exhibits the higher K values ($>1 \times 10^{-5}$ SI units) and very low $\mathbf{J}_n$ values ($0.01–0.03 \times 10^{-3}$ A/m with few inclusions). The PC-1–PC-2 boundary is more contrasting in Aksu-Dere, which is related to the hiatus. The section of the Submember XVIa in Kudrino-2 is much more complete; thus, its rock magnetic boundary is less striking. According to various parameters, it can be determined in the boundary range of Submembers XVIa and XVIb (from Sample 21 to Sample 24 inclusively). We combined the PC-2 base with the boundary of submembers (between Samples 22 and 23). This level is registered by the most significant increase in K values in the section and is additionally emphasized by increasing $\mathbf{J}_{rs}$ values (especially striking at the increase in the horizontal scale of the upper part of the plot). The typical changes in plots of rock magnetic parameters allowed the substantiation of some lithological boundaries. In particular, the boundary of Submembers XVIb and XVIc is marked by extremely low S values (0.5), which indicate the presence of a magnetically strong phase (probably, the oxidation products of pyrite), whereas the base of the Member XVId is registered by a typical minimum on the $K/\mathbf{J}_{rs}$ plot (Fig. 1a). The magnetic mineralogical characteristics of rock magnetic complexes are similar.

The magnetically soft minerals are magnetization carriers in samples. The remanent coercivity force (20–40 mT) and saturation field (~100 mT) in PC-1 rocks are typical of finely dispersed magnetite. Within PC-2, the $\mathbf{B}_{cr}$ (Figs. 1a, 1b) and $\mathbf{B}_s$ (Fig. 1b) values slightly increase, which is possibly due to the presence of Fe_3O_4 and other magnetic minerals, e.g., titanomagnetite.

The presence of magnetite is difficult to determine from TMA curves because of extremely low content of ferromagnetics. At high temperatures, a ferromagnetic signal becomes lower than the effect of the diamagnetic matrix, leading to negative values of induced magnetization. Nonetheless, some curves exhibit a weak bend in the area of the Curie temperature of Fe_3O_4 of 578°C (Fig. 1c).

An insignificant increase in magnetization at temperatures above 500–570°C, which is observed in all samples during the first or/and second heating (Fig. 1c), is most likely related to the reduction of Fe from magnetite. According to (Mikhailov et al., 2009), the heating of magnetite in a closed system with calcite and carbon (i.e., under conditions typical of our carbonate rocks) results in reduction of Fe. Regular release of

negligible (but surely registered) Fe contents is in agreement with a hypothesis on the presence of Fe_3O_4.

In contrast to PC-1, which possibly contains only magnetite according to TMA data, PC-2 hosts other ferromagnetic phases, which are registered by a small increase of magnetization in a range of 350 and 480°C (Fig. 1c). A weak increase in magnetization before the Curie temperature of the minerals is typical of titanomagnetite (Burov and Yasonov, 1979). A similar thermomagnetic effect is detected, e.g., in titanomagnetite from ash of volcanoes Bezymyanny in Kamchatka (Zubov and Kir'yanov, 2001), Mt. St. Helen in the Cascade Mountains, and Novarupta in Alaska (Jackson and Bowles, 2014). This and previous materials on the presence of a volcanic constituent in sections (Guzhikov et al., 2021) suggest an ash origin of our titanomagnetite.

The coercivity characteristics of samples from the Member XV (PC-1) on the Day plot (Fig. 1d) occur near the area of a theoretical curve corresponding to a pseudoeponymous magnetite (Dunlop, 2002). The samples from Submembers XVIb–XVId and the Member XVII (PC-2) poorly correspond to a standard plot, which can be explained by the presence of a magnetically strong phase in PC-2 (Fig. 1b).

The results of magnetic saturation, TMA, and coercimetry indicate that the finely dispersed magnetite is a main carrier of magnetization in the studied rocks, but the upper part of the section (PC-2) also contains magnetically strong ferromagnetics.

The indicator of magnetic anisotropy *P*, with rare exceptions, varies from 1 to 1.4, indicating almost isometric morphology of ferromagnetic particles. The indicator of morphology of magnetic grains (parameter *T*) registers the dominant flattened particles in PC-2. Thus, no regular orientation of short axes of magnetic ellipsoids is observed in contrast to PC-2, where they evidently group in the center of stereoprojection, which is typical of primary structures of sediments with dominant flat particles (Fig. 1f). The formation of sedimentary magnetic texture in Submembers XVIb–XVId and the Member XVII is possibly caused by the increase in the amount of clay particles, on the flat surface of which the finely dispersed ferromagnetics concentrate.

The high *Q* factor (1–5) of PC-1 (Fig. 1a) with high probability indicates a chemical genesis of magnetization. The low *Q* values (0.01–0.1) (Fig. 1a) together with magnetic texture similar to sedimentary origin (Fig. 1f) testify in favor of orientation (postorientation) genesis of $\mathbf{J}_n$ in PC-2.

The paleomagnetic studies were conducted following the method of (Molostovskii and Khramov, 1997), which included the measurement of $\mathbf{J}_n$ of oriented samples on a JR-6 spinner magnetometer after magnetic cleaning by an alternating field (from 5 to 50–100 mT with a step of 5 mT) on a LDA-3 AF device or temperature (from 100 to 550°C with a step of 50°C) in an oven of Aparin's construction. The possible phase transitions of minerals were controlled by the measurement of *K* values of samples after each thermal cleaning. Each of 109 sampled levels in the sections is characterized by 3–4 oriented samples in forms of cubes 2 × 2 × 2 cm in size (cut from hand specimens taken in the section using an entrenching tool) or cylinders 2.5 cm high and 2.2 cm in diameter (drilled directly from beds by a Drill Core D261-c driller). The paleomagnetic studies of samples from 30 different levels are repeated on a (SQUID) 2G-Enterprices cryogenic magnetometer at the IPE RAS, and the measurement results from two devices are well correlated (Fig. 2). The Remasoft 3.0 program was used for the component analysis (Chadima and Hrouda, 2006).

The paleomagnetic properties of PC-1 and PC-2 are distinct. The PC-1 rocks have good paleomagnetic quality. In spite of low magnetic susceptibility (mostly, $<2 \times 10^{-5}$ SI units), Submembers XVa–XVc in the Aksu-Dere section have relatively high $\mathbf{J}_n$ ($0.1–0.8 \times 10^{-3}$ A/m) and, thus, a high *Q* factor (1–4 and higher) (Fig. 1a). The characteristic remanent magnetization (ChRM) components are recognized in Submembers XVa–XVc, their corresponding maximum angle deviation (MAD) mostly ranges from 0.5° to 4°, and the rocks are mostly characterized by a one-component composition of $\mathbf{J}_n$. Submembers XVb–XVd and XVIa in the Kudrino-2 section (in the Aksu-Dere section, Submembers XVd and XVIa are strongly condensed) also have a sufficient paleomagnetic quality with two-component $\mathbf{J}_n$: low-coercivity (5–15 mT) or low-temperature (100–200°C) components possibly of a viscous origin ($\mathbf{J}_v$) and high-temperature (250–500°C) ChRM, the MAD of which is 4°–10° (Fig. 3).

All paleomagnetic directions in the Member XV and the Submember XVIa correspond to normal field polarity (Figs. 4a, 4b), excluding Sample 3168-40 in the Aksu-Dere section, which exhibits an anomalous vector of north direction with negative inclination

Fig. 1. Results of paleomagnetic, rock magnetic, and magnetic mineralogical studies of the Kudrino-2 and Aksu-Dere sections. (a) Magnetostratigraphic sections; (b) curves of magnetic saturation and decomposition; (c) TMA curves; (d) Day diagram (SD, PSD, and MD are the areas of single-domain, pseudo-one-domain, and multidomain particles, respectively); (e) diagram of parameters of magnetic anisotropy *P*–*T* (areas of positive and negative *T* values correspond to flattened and elongated forms of ferromagnetic particles, respectively); (f) stereographic schemes of concentration of short axes of ellipsoids of magnetic susceptibility in the paleogeographic coordinate system. 1–4, Geomagnetic polarity: 1, normal; 2, reversed; 3, 4, anomalous (distinguished by components $\mathbf{J}_n$, which are closer to the directions of direct and reversed polarity, respectively); 5, no polarity data; 6, levels, at which $\mathbf{J}_n$ during magnetic demagnetizations is shifted along the arches of large circles; 7–9, $\mathbf{J}_n$ components: 7, characteristic (ChRM); 8, viscous ($\mathbf{J}_v$); 9, stable ($\mathbf{J}_{st}$).

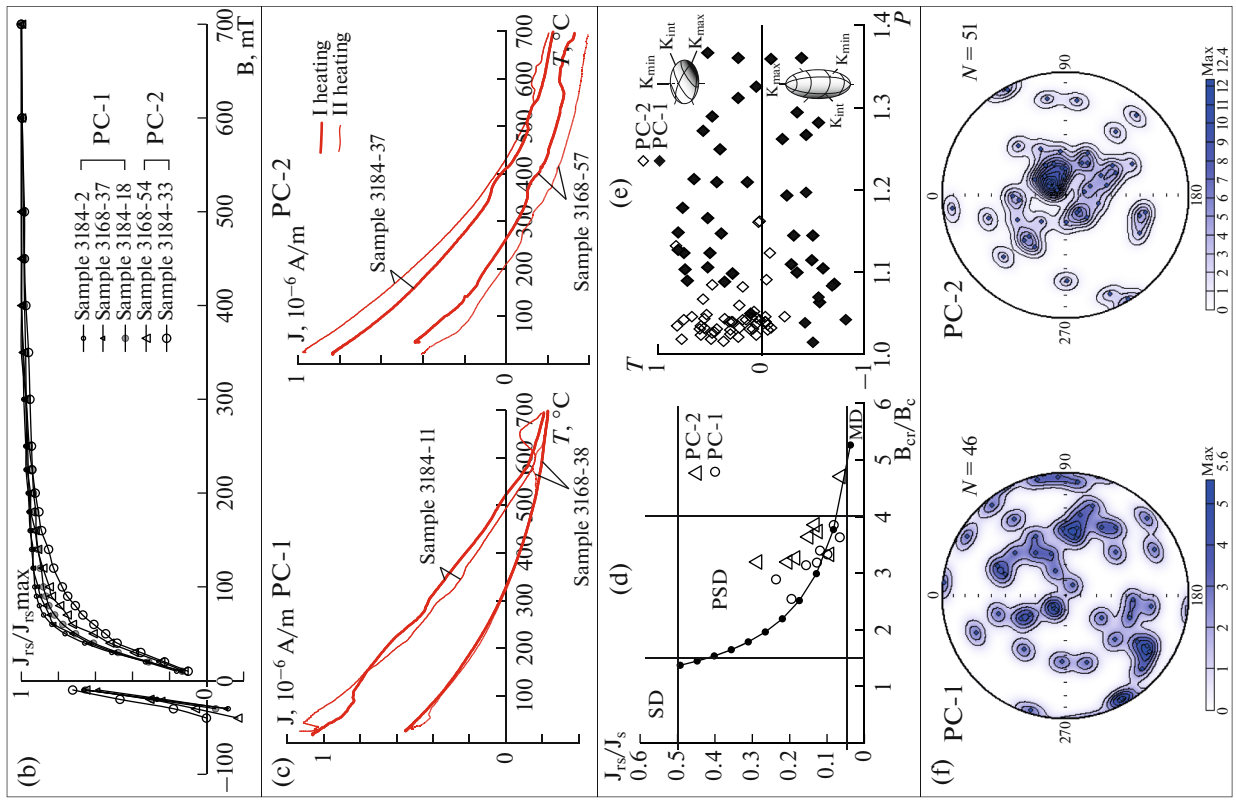
(b)
Sample 3184-2
Sample 3168-37
Sample 3184-18
Sample 3168-54
Sample 3184-33
PC-1
PC-2
B, mT
(c)
PC-1
PC-2
I heating
II heating
Sample 3184-11
Sample 3168-38
Sample 3184-37
Sample 3168-57
T, °C
(d)
SD
PSD
MD
PC-2
PC-1
(e)
PC-2
PC-1
(f)
PC-1
PC-2
N = 46
N = 51
Max

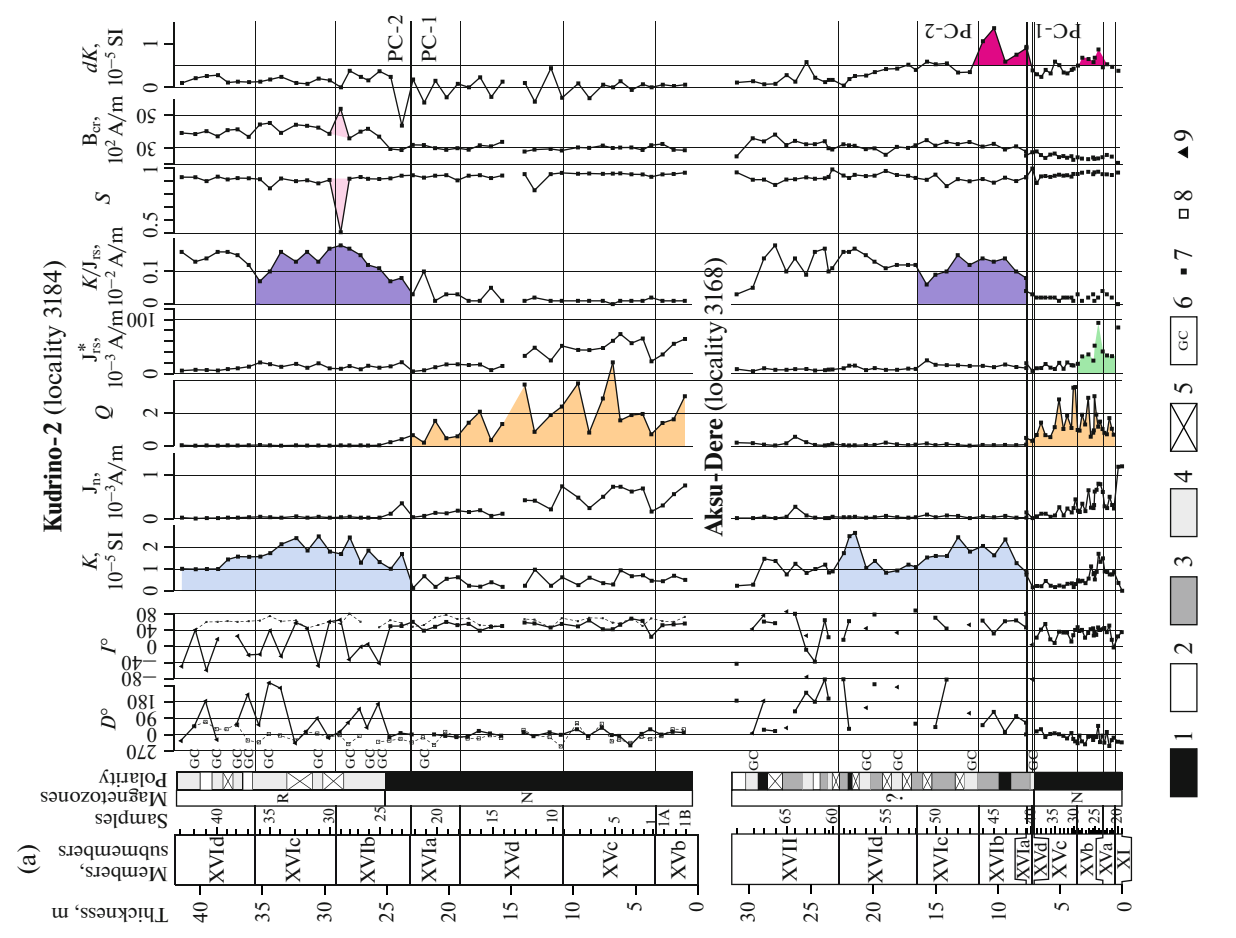
(a)
Kudrino-2 (locality 3184)
Aksu-Dere (locality 3168)
Thickness, m
Members, submembers
Samples
Magnetozones
Polarity
PC-1
PC-2
1 2 3 4 5 GC 6 7 8 9

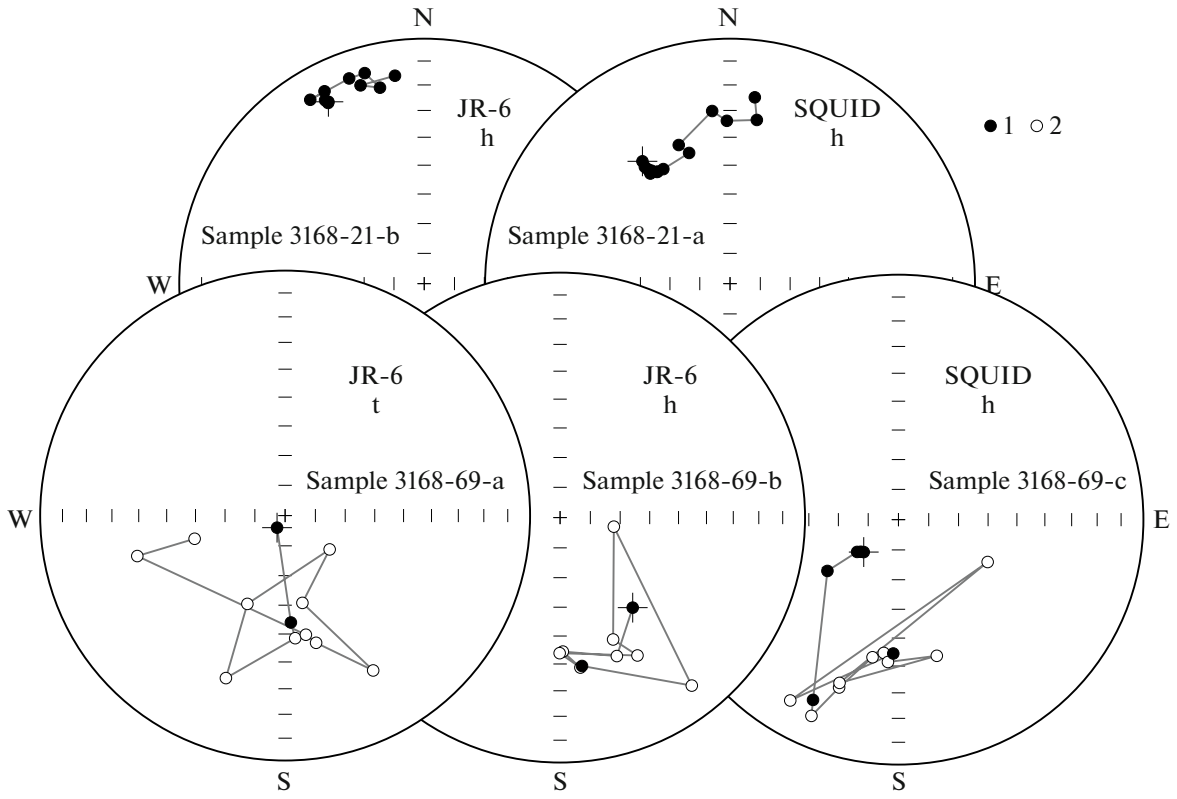

Fig. 2. Comparison of results of magnetic demagnetizations by an alternating field (h) and temperature (t) on a JR-6 spin-magnetometer at the Laboratory of Petrophysics of the Saratov State University (Saratov) and a 2G-Enterprices magnetometer (SQUID) at the IPE RAS (Moscow). The polar stereoprojections are given in stratigraphic coordinate system. 1, 2, projections of $\mathbf{J_n}$ on lower (1) and upper (2) semispheres.

(Submember XVIa in the Aksu-Dere section is only 0.5 m thick and an oriented hand specimen was taken from one level (Fig. 1a)).

Submembers XVa–XVc in the Aksu-Dere section are characterized by a high dispersion of ChRM directions (Fig. 4b). Similar anomalous dispersion is typical of the underlying Turonian–Coniacian rocks of the Aksu-Dere section, which were studied before (Guzhikov and Feduleev, 2019). In younger rocks composing Submembers XVd and XVIa in the Kudrino-2 section, no similar high-amplitude variations are observed. The average ChRM direction in them is similar to the directions which were recognized in the Upper Cretaceous (in the upper parts of the Campanian–Maastrichtian) of Southwestern Crimea (Baraboshkin et al., 2020; Guzhikova, 2019) in contrast to the average direction with strongly decreased inclination in Submembers XVa–XVc of the Aksu-Dere section (Fig. 4b, Table 1). This event cannot be explained by reasons having no relation to an ancient geomagnetic field (such as partial remagnetization, synfold deformations, etc.). Thus, this stage of the studies also considers a hypothesis (together with others) of the presence of previously unknown high-amplitude field variations in the Coniacian and Santonian (Guzhikov and Feduleev, 2019).

The paleomagnetic quality of PC-2 rocks is worse in comparison with PC-1 rocks. In the Kudrino-2 section, the characteristic components of normal polarity with high MAD values (14°–15°) are reliably recognized in the base of PC-2 (Samples 23–24), as well as in the underlying rocks. Up the section, in addition to viscous magnetization, one can also recognize one more component, which is not characteristic (Fig. 1a). These components (conditionally, "stable" ($\mathbf{J_{st}}$) are projected on northern rhumbs of the lower hemisphere and the upper hemisphere; some of them are characterized by directions typical of normal or reverse polarity (Fig. 4c). In many samples, the projections $\mathbf{J_n}$ are shifted along the arcs of a great circle (GC) during remagnetization (Fig. 3), which is related to the presence of variously directed components of remagnetization. Stable components are most likely the stabilized sums of two antiparallel components: primary, corresponding to the reverse polarity, and secondary, related to the present-day field. The different degree of "contamination" of the total magnetization by viscous component results in high dispersion of $\mathbf{J_{st}}$ in

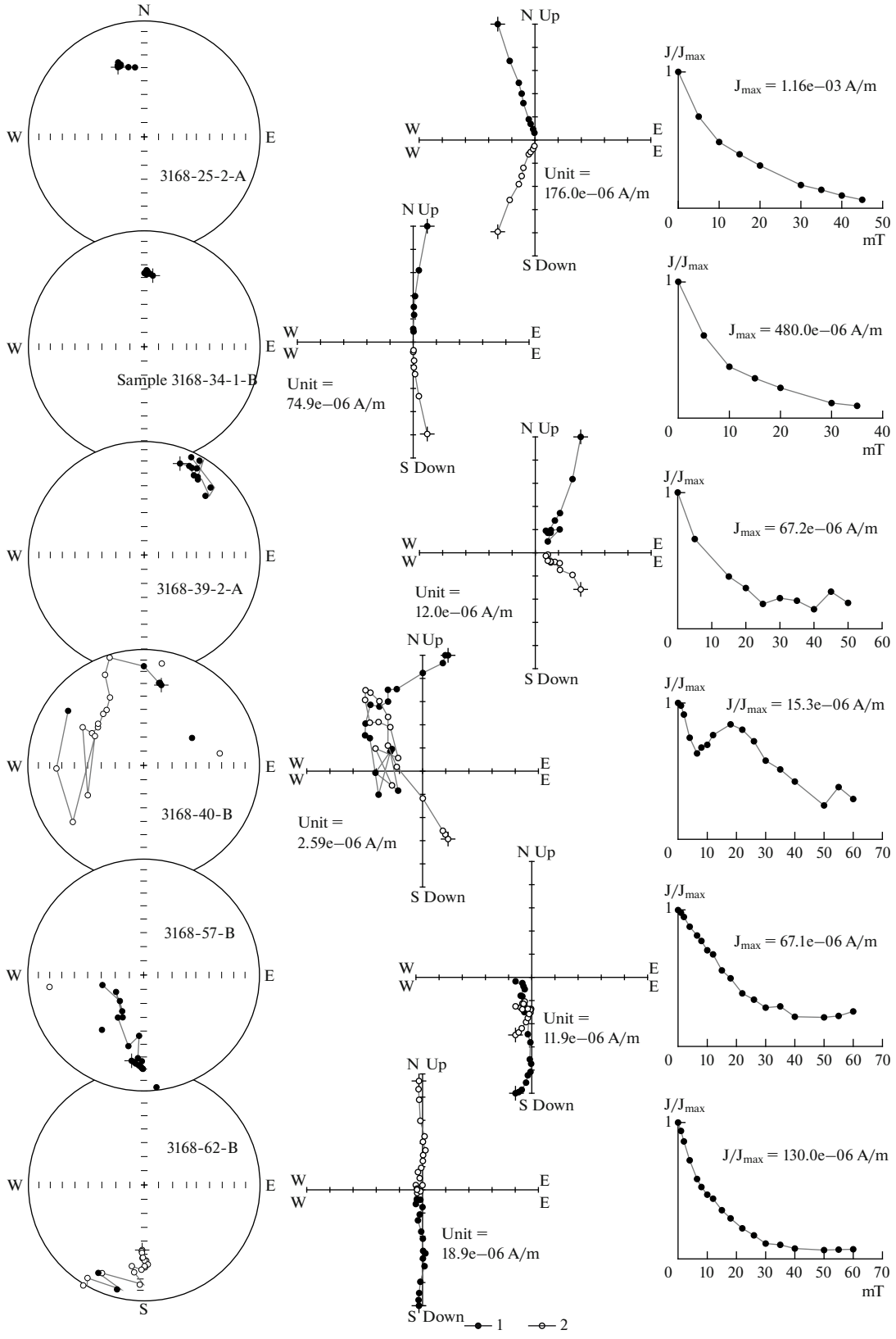

Fig. 3. Results of the component analysis (from left to right): images on polar stereoprojections of changes in $\mathbf{J_n}$ vectors during magnetic demagnetizations (in stratigraphic coordinate system); Zijderveld diagrams (in stratigraphic coordinate system); plots of demagnetization of samples. 1, 2, projections of $\mathbf{J_n}$ on horizontal (1) and vertical (2) planes. For other symbols, see Fig. 2.

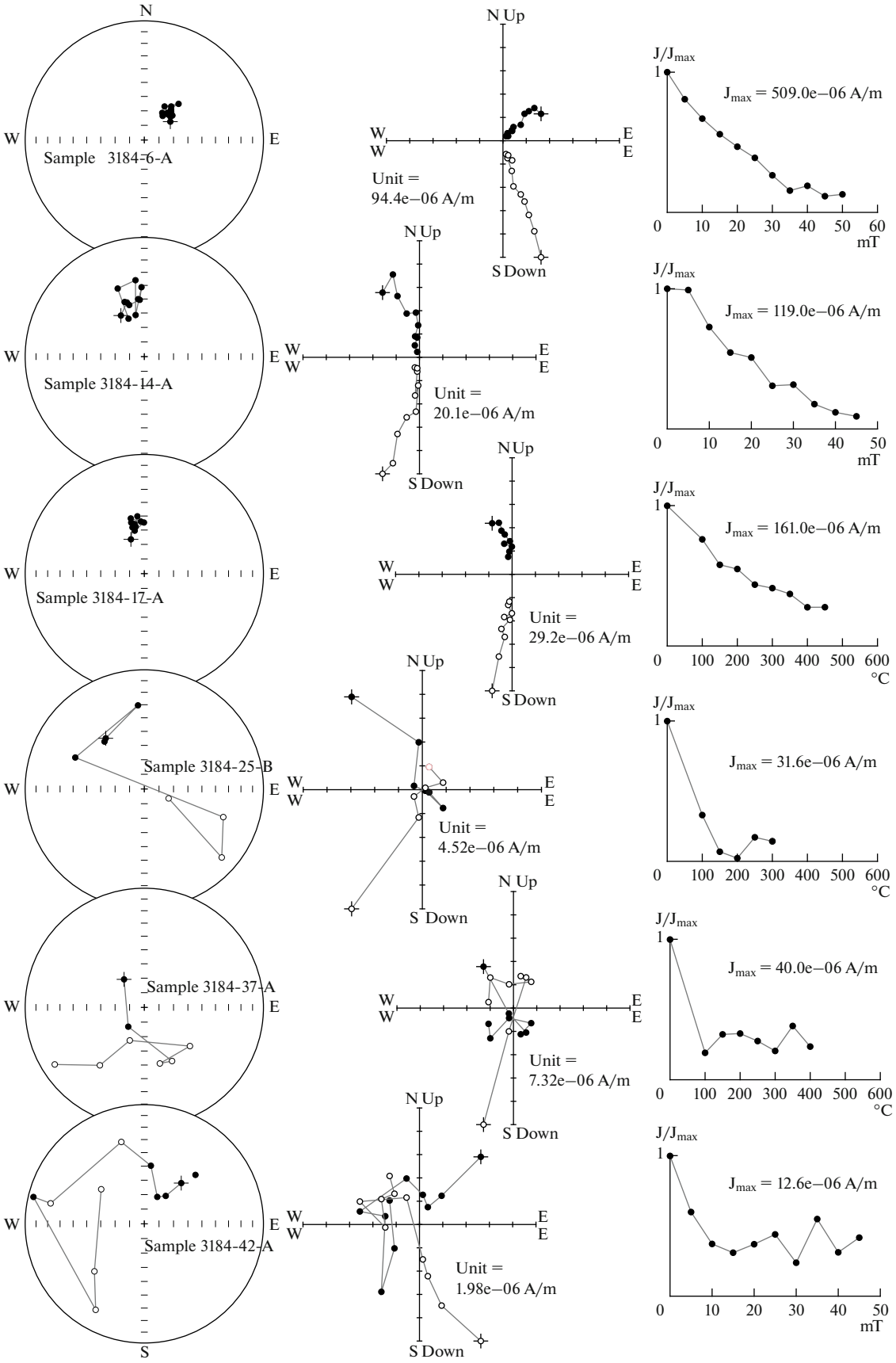
N
W
E
S
Sample 3184-6-A
Sample 3184-14-A
Sample 3184-17-A
Sample 3184-25-B
Sample 3184-37-A
Sample 3184-42-A
N Up
S Down
Unit = 94.4e–06 A/m
Unit = 20.1e–06 A/m
Unit = 29.2e–06 A/m
Unit = 4.52e–06 A/m
Unit = 7.32e–06 A/m
Unit = 1.98e–06 A/m
J/Jmax
Jmax = 509.0e–06 A/m
Jmax = 119.0e–06 A/m
Jmax = 161.0e–06 A/m
Jmax = 31.6e–06 A/m
Jmax = 40.0e–06 A/m
Jmax = 12.6e–06 A/m
mT
°C

Fig. 3. (Contd.)

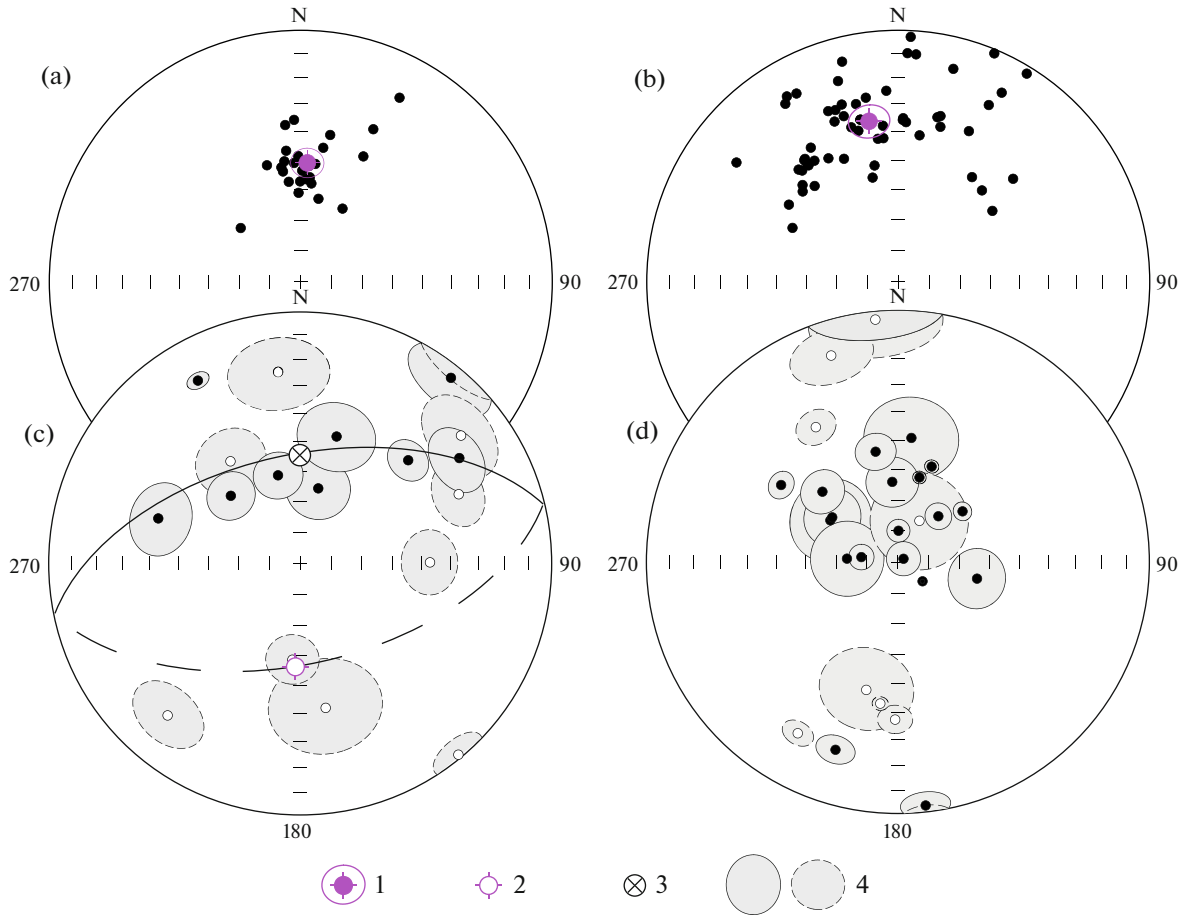

Fig. 4. Polar stereoprojections of $\mathbf{J_n}$ components in stratigraphic coordinate system. (a), (b), ChRM, by which *N*-zones are recognized in the Kudrino-2 and Aksu-Dere sections, respectively; (c), $\mathbf{J_{st}}$, which correspond to *R*-zone in the Kudrino-2 section; (d) $\mathbf{J_{st}}$ and ChRM in interval of the Aksu-Dere section without magnetozone. 1, Average paleomagnetic direction and radius of 95% confidence circle for it; 2, hypothetical average paleomagnetic direction corresponding to reversed polarity (opposite to the average ChRM direction for normal polarity); 3, average direction of demagnetization by current field; 4, maximum angle deviations (MAD) for $\mathbf{J_n}$ projections to lower and upper (dotted line) semispheres. For other symbols, see Fig. 2.

the case of the opposite sign of ancient magnetization and less affects the paleomagnetic statistic by primarily normally magnetized samples because of similar directions of the present-day and Late Cretaceous normal fields.

In the upper parts of the Kudrino-2 sections, the character of paleomagnetic data agrees with a model of partial preservation of opposite sign, the average direction of which differs by 180° from the average ChRM direction corresponding to normal polarity. The distribution of "stable" components on stereoprojections tends to larger circle, which follows the direction of remagnetization of rocks by the present-day field and ChRM (Fig. 4c). Thus, we can suggest that a magnetozone of reverse polarity corresponds to the Submember XVIb (except for its lower parts) and Submembers XVIc and XVd (Fig. 1a).

A similar paleomagnetic scenario is observed in PC-2 of the Aksu-Dere section (Members XVI–XVII; Figs. 1a, 3, 4d). The abundance of $\mathbf{J_{st}}$ and ChRM, which are projected with steep inclinations on the lower hemisphere in northern rhumbs (Fig. 4d), however, forces us to refrain from magnetopolar interpretation of data in this part of the section. Thus, the paleomagnetic column of the Aksu-Dere section contains only one magnetozone of normal polarity (*N*), which corresponds to Submembers XVa–XVc (Fig. 1a), whereas the presence of an overlying magnetozone of reverse sign can only be suggested by analogy with members of the same age in the Kudrino-2 section.

The paleomagnetic column of the Kudrino-2 section consists of two magnetozones: lower and upper of normal (*N*) and reversed (*R*) polarity, respectively, the boundary between which occurs at the level between Samples 24 and 25 (Fig. 4a). The normal polarity zone in the Aksu-Dere section partly overlaps the *N* zone identified in the Kudrino-2 section and increases it to the base (Fig. 1a).

It is impossible to apply the standard field tests to our materials. The reverse test is excluded because the

Table 1. Statistical paleomagnetic parameters

			n	D_{av}°	I_{av}°	k	α_{95}°	Φ°	Λ°	A_{95}°	φ_{m}°
Aksu-Dere (locality 3168) *N-zone*	Geo	60	355.5	44.5	10.7	5.9					
	Tilt		350.0	35.6	10.7	5.9	63.7	235.6	9.4	19.7
Kudrino-2 (locality 3184) *N-zone*	Geo	26	19.6	58.9	32.6	5.0					
	Tilt		3.1	50.9	32.6	5.0	76.6	211.6	5.6	31.6
Steady Europe (Besse and Courtillot, 2002)	80 Ma (averaging of 10 Ma)						81.4	206.1	5.9	
	85 Ma (averaging of 5 Ma)						81.0	230.5	10.3	
	90 Ma (averaging of 10 Ma)						82.2	202.1	5.2	
SW Crimea	Maastrichtian Chakhmakhly and Takma sections (Guzhikova, 2019)						73.2	246.1	4.2	30.0
	Mt. Beshkosh, Campanian–Maastrichtian (Baraboshkin et al., 2020)						77.9	241.2	4.0	33.8
CC	Mt. Alan-Kyr, Santonian–Campanian (Guzhikov et al., 2020a)						59.0	125.9	10.6	36.8

Geo and Tilt, geographic and stratigraphic coordinate systems, respectively; n, number of samples; D_{av} and I_{av}, average declination and inclination of ChRM, respectively; k, interbed precision parameter; α_{95}, radius of confidence circle of vector; Φ, Λ, and A_{95}, latitude, longitude, and radius of confidence circle of paleomagnetic pole, respectively; φ_m, paleolatitude. Table provides the poles for steady Europe with age, which is the closest to the modern age of the Santonian–Campanian boundary of 83.65 Ma (Gradstein et al., 2020), as well as for Upper Cretaceous of Crimea. CC, Central Crimea.

materials which are the basis for the recognition of the *R* zone (Figs. 1a, 4c) are unsuitable for the calculation of the paleomagnetic statistic, the variations in bedding elements in sections are too low for the fold test, and there is no evidence to apply the conglomerate tests. The primary character of $\mathbf{J}_n$ can be judged from several indirect features which are widely used in magnetostratigraphy for the substantiation of the age of magnetization (Guzhikov, 2013):

(1) The ranges of the same sign of polarity are grouped along the section and form large *N* and *R* magnetozones (Fig. 1a).

(2) No correlation between the sign of polarity and the composition and physical properties of rocks is a feature of ancient nature of $\mathbf{J}_n$, whereas the correlation of magnetozones with a certain type of rocks suggests a possible remagnetization. The presence of similar correlation can only be verified in the Kudrino-2 section because of only one magnetozone in the Aksu-Dere section. The paleomagnetic boundary in the Kudrino-2 section apparently corresponds to the level of sharp rock magnetic changes; however, the base of the *R* zone does not coincide with the boundary of the rock magnetic complexes. Irrespective of what rock magnetic parameter is responsible for the identification of the PC-2 base, it always occurs several meters below the top of the *N* zone. Even in its highest position, which is determined by the increase in magnetic susceptibility, the lower parts of PC-2 have normal polarity (Samples 23 and 24). It is important from the viewpoint of evidence of primary character of $\mathbf{J}_n$ that the MAD in these samples increases to critical values of 14°–15°. Thus, the change in sedimentation conditions (Guzhikov et al., 2021), which is also registered by geochemical parameters (see section "Isotopic–Geochemical Characteristics) and the new magnetization carriers (most likely, titanomagnetite from volcanic ash) are accompanied by decreasing paleomagnetic quality of rocks rather than the change in the sign of polarity. It is likely that Samples 23 and 24 at the base of PC-2 (as well as in Samples 21 and 22 at the top of PC-1) underwent less remagnetization than the overlying rocks covered by the *R* zone, whereas their ChRM is also a stabilized sum of primary and secondary components. The effect of remagnetization in them is invisible because of similar directions of the ancient and present-day field of normal polarity.

(3) The high (in comparison with sedimentary rocks) values of the *Q* factor (1–4 and more) decreasing up the section are typical of PC-1 (Fig. 1a). This is atypical of the orientation (postorientation) nature of magnetization, but it is typical of the chemical genesis of $\mathbf{J}_n$. The results of previous magnetic mineralogical and microprobe studies of samples from the Member XI and Submembers XVa–XVc indicate the presence of biogenic magnetite (Guzhikov and Feduleev, 2019), which proves the primary magnetization. Other scenarios of the origin of Fe_3O_4 (cosmogenic (meteorite dust) or chemogenic (due to migration of hydrocarbons from a layer of bitumen shales located below in the section, at the border of the Cenomanian–Turonian)) are unlikely.

The presence of components $\mathbf{J}_n$ with anomalous or reversed directions and the shift of paleomagnetic vectors during magnetic demagnetization along the arcs of great circles are consistent with a hypothesis on the presence of ancient components $\mathbf{J}_n$ reversed polarity which are partly remagnetized by the present-day field.

(4) The paleomagnetic pole, which is calculated by the normal direction of ChRM in the Kudrino-2 section, statistically coincides with poles for stable Europe similar in age (Table 1). This circumstance neither excludes the primary magnetization nor proves it. According to Pechersky and Safonov (1993), the Mountainous Crimea after the Early Cretaceous moved to the north together with the East European Platform and Scythian Plate. At the same time, the pole along the Kudrino-2 section somewhat (but significantly) differs from the poles by the upper parts of the Campanian–Maastrichtian of the Southwestern Crimea and strongly differs from the pole by rocks of Central Crimea of the same age (Table 1), which can be related to local displacements of blocks relative to each other. We also should mention consistent (with consideration of the proportion) paleolatitudes of the Campanian–Maastrichtian of Southwestern Crimea with current ideas on the position of the Mountainous Crimea in the Late Cretaceous (Pechersky and Safonov, 1993).

The average paleomagnetic pole and paleolatitude calculated by ChRM in the Aksu-Dere section (Submembers XVa–XVc) contradict all known data. Because the remagnetization of rocks is unlikely, the anomalous ancient geomagnetic field remains the most possible reason for the high ChRM dispersion.

(5) Our paleomagnetic data correspond to the criterion of external convergence; i.e., they agree with current ideas on a magnetopolar structure of the Santonian–Campanian boundary (Gradstein et al., 2020). The *N* and *R* zones are easily recognized as analogs of the upper parts of chrons 34n and the lower parts of chron 33r, respectively.

All these features, each of which largely fits a hypothesis on ancient origin of $\mathbf{J_n}$ rather than a hypothesis on its secondary genesis, testify in favor of the idea that this succession of magnetozones reflects the regime of the geomagnetic field at the Santonian–Campanian boundary. These data meet five criteria of eight which are accepted for the estimation of reliable magnetostratigraphic materials. This is sufficient to acknowledge their quality (*Dopolneniya...*, 2000).

ISOTOPIC–GEOCHEMICAL CHARACTERISTICS

The authors present the new results of the comprehensive isotopic–geochemical study of the Santonian–Campanian carbonate rocks of the Kudrino-2 and Aksu-Dere sections (Table 2). The Ca, Mg, Fe, Mn, and Sr contents and C and O isotopic composition are determined in 31 samples: 11 from locality 3168 (Aksu-Dere) and 20 from locality 3184 (Kudrino-2). The Sr isotopic composition is analyzed in 18 samples: 8 from locality 3186 (Aksu-Dere) and 10 from locality 3184 (Kudrino-2).

The Ca, Mg, Fe, Mn, and Sr contents are determined in the carbonate part of rock after dissolution of 30–35 mg of a powdered sample in a 0.6 N HCl solution. The contents were analyzed on an ICPE-9000 atomic emission spectrometer (MACB, St. Petersburg State University, St. Petersburg). Noncarbonate material remains after dissolution in 0.6 N HCl solution. According to X-ray analysis, it is composed of quartz and clay minerals. The contents of major and trace elements are recalculated taking into account the amount of silicates.

The C and O isotopic composition was measured on a Delta V Advantage mass spectrometer equipped with a GasBench II device (Center for Collective Use Geonauka, Institute of Geology, Komi Science Center, Ural Branch, Russian Academy of Sciences). The $\delta^{13}C$ and $\delta^{18}O$ values are given in per mille relative to the V-PDB standard (Table 2). The international standards NBS-18 and NBS-19 are used for calibration. The measurement error is ±0.15‰ (1σ).

The Sr isotopic composition of carbonate rocks is analyzed using stepped dissolution including preliminary treatment of a sample ~30 mg in weight by 0.01 N HCl solution and further dissolution in 1 N HCl. Strontium was released from chemical solutions by chromatography (Kuznetsov et al., 2006). The Sr isotopic composition was measured on a Triton TI multicollector mass spectrometer. The average $^{87}Sr/^{86}Sr$ value in the standard sample NIST SRM 987 was 0.71025 ± 0.00001 ($2\sigma_{average}$, $n = 5$).

All studied samples of limestones, mostly composed of calcite (Mg <0.3%) with a widely variable amount of silicates (from 0.7 to 19.8%) demonstrate rhythmicity (Table 2, Fig. 5). The terrigenous content in limestones of the Member XI is 6–7%, then sharply increases in the base of the Member XV to 16–18%, and gradually decreases toward the top of this member to 5–8%. The amount of terrigenous material in Member XVI increases from 1–2 to 10–19%.

The lowest contents of Mn (115–157 ppm), Fe (360–420 ppm), and Sr (370–510 ppm) are typical for limestones of Member XI of the Aksu-Dere section. In the Member XV, the Mn content of limestones decreases from 320 to 210 ppm, and the Fe content is constantly high (560–800 ppm), whereas the Sr content increases from 516 to 620 ppm in the Aksu-Dere section and from 415 to 535 ppm in the Kudrino-2 section. In the Member XVI, the Mn content increases from 220–240 to 320 ppm, whereas the Fe and Sr contents are extremely high and reach 890–1250 and 600–720 ppm, respectively.

The $^{87}Sr/^{86}Sr$ value of limestones of the Member XI varies from 0.70741 to 0.70744 (Table 2, Fig. 5). In Submember XVa, it is 0.70744–0.70747, increasing up the section: 0.70744–0.70752 in Submember XVb, 0.70750–0.70752 in Submembers XVc and XVd, and 0.70750–0.70755 in the Member XVI.

Table 2. Trace element contents, amount of silicates (s.), and $^{87}Sr/^{86}Sr$, $\delta^{13}C$, and $\delta^{18}O$ values of the Upper Cretaceous limestones in Aksu-Dere and Kudrino-2 sections

Samples	Member	Amount of s., %	Ca, %	Mg, %	Mn, ppm	Fe, ppm	Sr, ppm	Mn/Sr	Fe/Sr	$\delta^{13}C$, ‰ PDB	$\delta^{18}O$, ‰ PDB	$^{87}Sr/^{86}Sr$
Aksu-Dere												
3168/17A	XI	5.9	40.4	0.2	115	425	370	0.31	1.1	3.0	–2.5	0.70741
3168/18A	XI	7.1	40.3	0.2	124	370	510	0.24	0.7	3.1	–4.1	0.70744
3168/19A	XI	7.1	40.2	0.2	150	360	480	0.33	0.8	3.2	–3.6	
3168/21A	XVa	15.7	41.3	0.2	305	650	516	0.59	1.3	2.5	–3.9	0.70745
3168/22A	XVa	18.2	40.2	0.2	320	790	530	0.61	1.5	2.6	–4.6	0.70747
3168/23A	XVb	15.0	38.4	0.2	310	725	540	0.58	1.3	2.9	–3.8	0.70744
3168/24A	XVb	13.8	40.6	0.2	309	605	560	0.55	1.1	2.9	–4.1	
3168/26A	XVb	16.5	39.9	0.2	286	710	640	0.45	1.1	2.7	–4.3	0.70748
3168/27A	XVb	12.9	37.5	0.2	246	564	556	0.44	1.0	2.6	–2.9	
3168/28A	XVb	9.9	39.6	0.2	250	605	590	0.43	1.0	2.9	–3.5	0.70752
3168/29A	XVc	15.0	40.8	0.2	260	580	620	0.41	0.9	2.8	–4.5	0.70751
Kudrino-2												
3184/1A	XVb	8.6	39.8	0.3	260	760	420	0.61	1.8	2.7	–4.3	
3184/1	XVc	8.2	39.5	0.2	275	660	415	0.66	1.6	2.4	–2.7	0.70750
3184/5	XVc	7.1	40.6	0.2	224	636	480	0.46	1.3	2.7	–4.3	0.70751
3184/6	XVc	0.7	39.5	0.2	244	700	470	0.52	1.5	2.6	–3.9	
3184/7	XVc	5.2	40.0	0.2	218	775	516	0.42	1.5	2.6	–3.6	0.70751
3184/9	XVc	5.6	39.6	0.2	237	670	510	0.46	1.3	2.6	–3.9	
3184/11	XVd	8.9	39.2	0.2	210	720	510	0.42	1.4	2.7	–4.1	0.70752
3184/15	XVd	6.4	40.0	0.2	240	680	535	0.45	1.3	2.7	–3.8	
3184/19	XVIa	1.7	39.6	0.2	248	710	556	0.45	1.3	3.0	–4.3	0.70750
3184/20	XVIa	2.4	39.9	0.2	274	715	540	0.51	1.3	3.1	–4.2	
3184/24	XVIb	13.4	39.7	0.2	240	1100	590	0.41	1.9	2.9	–4.5	0.70753
3184/26	XVIb	10.6	39.7	0.3	220	1090	624	0.36	1.7	3.1	–3.8	
3184/29	XVIb	12.7	39.9	0.3	248	1195	720	0.34	1.7	2.9	–3.6	0.70752
3184/31	XVIc	19.4	39.8	0.3	269	1226	680	0.39	1.8	2.9	–3.5	
3184/32	XVIc	10.1	39.7	0.3	274	1250	700	0.39	1.8	2.9	–3.6	
3184/34	XVIc	13.6	39.5	0.3	270	1205	670	0.41	1.8	2.8	–4.4	0.70753
3184/37	XVId	12.9	39.8	0.3	304	1020	640	0.48	1.6	2.8	–3.6	
3184/40	XVId	6.2	39.0	0.3	297	890	660	0.45	1.3	3.1	–6.1	0.70755
3184/42	XVId	13.2	39.2	0.3	308	995	646	0.48	1.5	3.0	–4.9	
3184/43	XVId	19.8	39.3	0.2	310	990	670	0.46	1.5	2.5	–6.2	0.70752

The $\delta^{13}C$ value of limestones varies from 2.4 to 3.2‰, whereas the $\delta^{18}O$ value ranges from –6.2 to –2.7‰ (Table 2). According to $\delta^{13}C$ values, three ranges can be distinguished in limestones, which is consistent with lithological subdivisions. The $\delta^{13}C$ values of Members XI, XV, and XVI are 3.0–3.2, 2.4–2.9, and 2.9–3.1‰, respectively (Table 2).

The $^{87}Sr/^{86}Sr$ ratio of limestones of the Member XV has generally a negative correlation with the Mn/Sr ratio and a positive correlation with the Fe/Sr ratio. This differs from the normal positive correlation between these parameters which is observed during epigenetic recrystallization of limestones as a result of impact of underground fluids and surface waters (Kuznetsov et al., 2005, 2006). The various trends of correlations of the $^{87}Sr/^{86}Sr$ values with the Mn/Sr and Fe/Sr ratios indicate much more complex diagenetic evolution of carbonate rocks in the Kudrino-2 and Aksu-Dere sections.

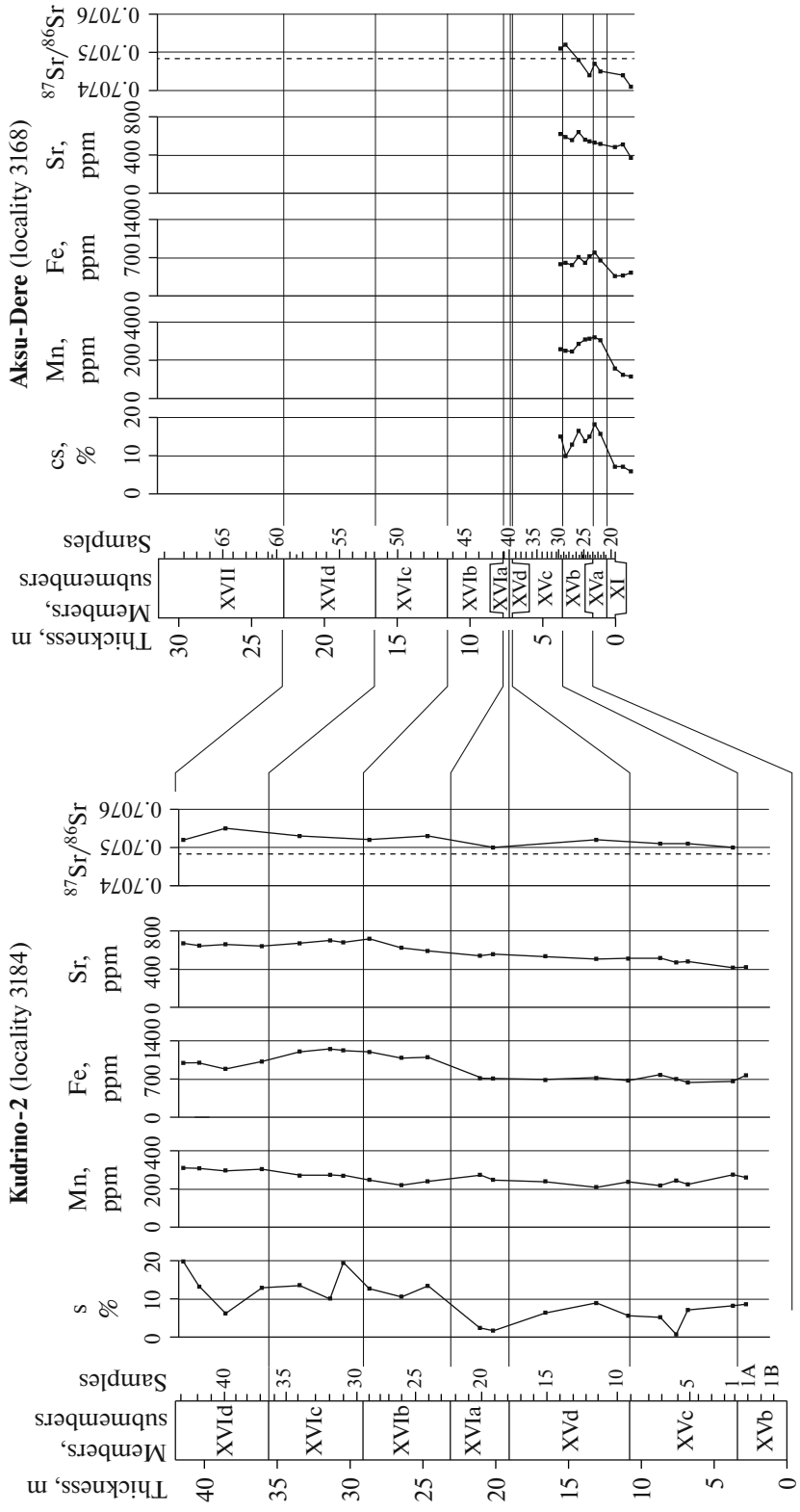

Fig. 5. Variations in amount of silicates (s.), Mn, Fe, and Sr contents, and $^{87}Sr/^{86}Sr$ ratio in the Kudrino-2 and Aksu-Dere sections. The dotted line corresponds to the $^{87}Sr/^{86}Sr$ value at the Santonian–Campanian boundary (McArthur et al., 2012).

Unfortunately, the studied samples do not fully meet geochemical parameters of preservation for the selection of the Mesozoic limestones during estimation of the Sr isotopic composition of seawater (Jones et al., 1994; Kuznetsov et al., 2017). For example, the values of geochemical parameters for less altered Upper Jurassic limestones of the Baidar Basin and Demerdzhi Plateau are as follows: Mg/Ca < 0.03, Mn/Sr < 0.2, Fe/Sr < 1.5 (Rud'ko et al., 2014, 2017). In the Aksu-Dere and Kudrino-2 sections, the Fe/Sr values in half of the sampling (17 samples) are ≥ 1.5, and the Mn/Sr values are higher in all samples, varying from 0.24–0.66 (Table 2). The carbonate rocks are probably partly enriched in Fe and, especially, Mn during the interaction with surface waters in the course of tectonic uplift of sequences (Kuznetsov et al., 2006; Rud'ko et al., 2014, 2017). It cannot be excluded that the repeated sampling at a significant distance from the day surface allows us to recognize the samples with inviolate Sr isotopic systems.

The $\delta^{18}O$ values (from –6.2 to –2.7‰) of studied limestones are lower than those of the Mesozoic marine carbonates of Tethyan paleobasins (from –2 to 0‰). The $\delta^{18}O$ and $\delta^{13}C$ values, however, show no correlations either with each other or with the Mn/Sr and Fe/Sr ratios. This fact indicates the absence of epigenetic recrystallization and the involvement of atmospheric waters (Pokrovskii et al., 2020). All limestones meet geochemical parameters of preservation for the selection of samples with intact C isotopic systems (Jones et al., 1994; Kuznetsov et al., 2006; Rud'ko et al., 2014, 2017; Semikhatov et al., 2004). The $\delta^{13}C$ values are consistent with similar values of the Mesozoic marine carbonates of the Tethyan paleobasins (Wagreich et al., 2010; Wendler, 2013; Zakharov et al., 2013).

The variations in $\delta^{13}C$ values in the combined Kudrino-2–Aksu-Dere section exhibit, at least, two positive excursions: lower in the Member XI of the Aksu-Dere section (the Coniacian Stage) and upper in the Submember XVIa of the Kudrino-2 section near the suggested Cantonian–Campanian boundary (Fig. 6).

DISCUSSION

Comparison of Studied Sections According to Comprehensive Data

The paleontological, paleomagnetic, and isotopic–geochemical data mostly agree with the detailed division and correlation of studied sections by lithological and rock magnetic data (Fig. 6) and the available differences can be explained. The results of the analysis of planktonic and benthic foraminifers (PF and BF, respectively) are in agreement with lithological-rock magnetic correlation of sections and promote its specification (Fig. 6).

The boundary of the UC13 and UC14 zones by nannoplankton in the studied sections is confined to various lithological subdivisions: Submembers XVd and XVc in the Kudrino-2 and Aksu-Dere sections, respectively (Fig. 6). Because of poor nannofossil assemblages in the Kudrino-2 section, the base of UC14 is conditional (see chapter "Nannoplankton" in (Guzhikov et al., 2021)) and probably occurs below the section.

The materials on dinocysts can agree with results of lithological–rock magnetic comparisons of the sections if the DK-1 assemblage (Submembers XVIa–XVIc in the Kudrino-2 section) is an analog of DAD-2 (Submembers XVIa–XVIc in the Aksu-Dere section). The dating of both assemblages by the end of the Santonian–the beginning of Campanian allows this; however, the trend of warming of waters, which is identified in Aksu-Dere by the decreasing amount of *Chatangiella* and *Isabelidinium* up the section, provides a basis to consider that DAD-2 is younger than DK-1 (see section "Palynology" in (Guzhikov et al., 2021)). The few data on dinocysts by four levels in the Aksu-Dere section and, in fact, by three levels of the Kudrino-2 section, however, are insufficient for unambiguous conclusions on the different age of DAD-2 and DK-1. Thus, changes in lithological–rock magnetic correlation of the sections on the basis of palynological materials is premature.

The paleomagnetic data are consistent with this scenario of correlation of sections, but they cannot refine it. In the Aksu-Dere section, Members XVI–XVII are mostly remagnetized (see section "Magnetostratigraphy"); however, the age of their formation corresponds to chron 33r with high probability, the analogs of which are identified in the Kudrino-2 section (Fig. 6).

The detailed correlation of sections by complex data supports a significantly more complete volume of Submembers XVb–XVIa of the Kudrino-2 section relative to the Aksu-Dere section and allows the composition of a summarized bio-, chemo-, and magnetostratigraphic section of the Santonian–Campanian boundary of Kudrino–Aksu-Dere (Fig. 6).

Comparison of the Santonian–Campanian Boundary of Southwestern and Central Crimea

The first (and still only) comprehensive micropaleontological (nannoplankton, dinocysts, PF, BF) and magnetostratigraphic data on the Santonian–Campanian of Central Crimea are available for the section of Alan-Kyr Mt. near the town of Belogorsk (Guzhikov et al., 2019; Kopaevich et al., 2020; Ovechkina et al., 2021). They showed another pattern in combination with micropaleontological and paleomagnetic results compared to Southwestern Crimea (Fig. 7).

The scenarios of the detailed correlations of the Santonian–Campanian boundary of Southwestern and Central Crimea by PF, BF, nannoplankton, and dinocysts contradict each other (Fig. 7). The reasons are related to diachronous biostratigraphic boundaries due to facial correlation of micropaleontological

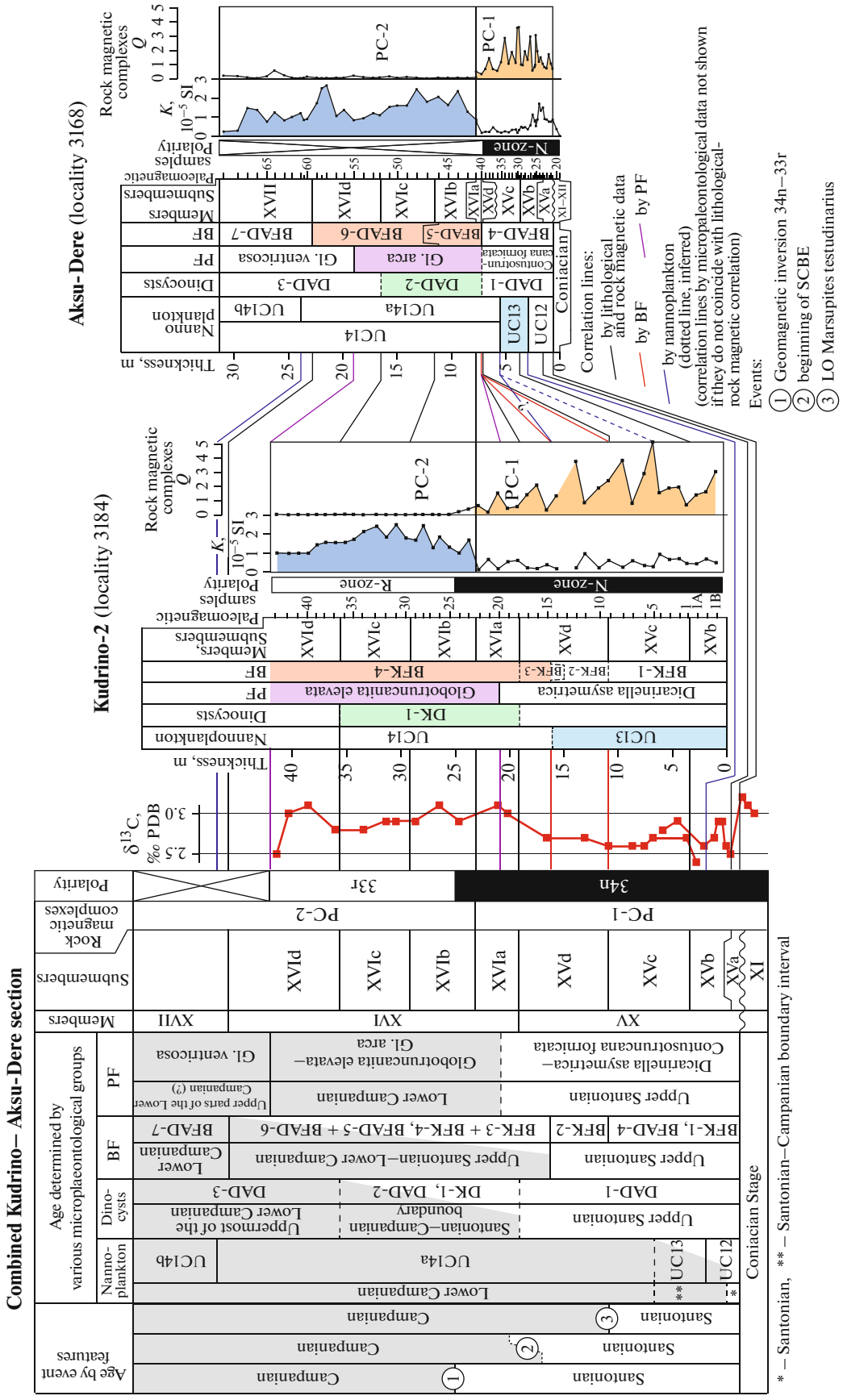

Fig. 6. Combined Kudrino– Aksu-Dere section of the Santonian–Campanian boundary, which are identified by various methods and events.

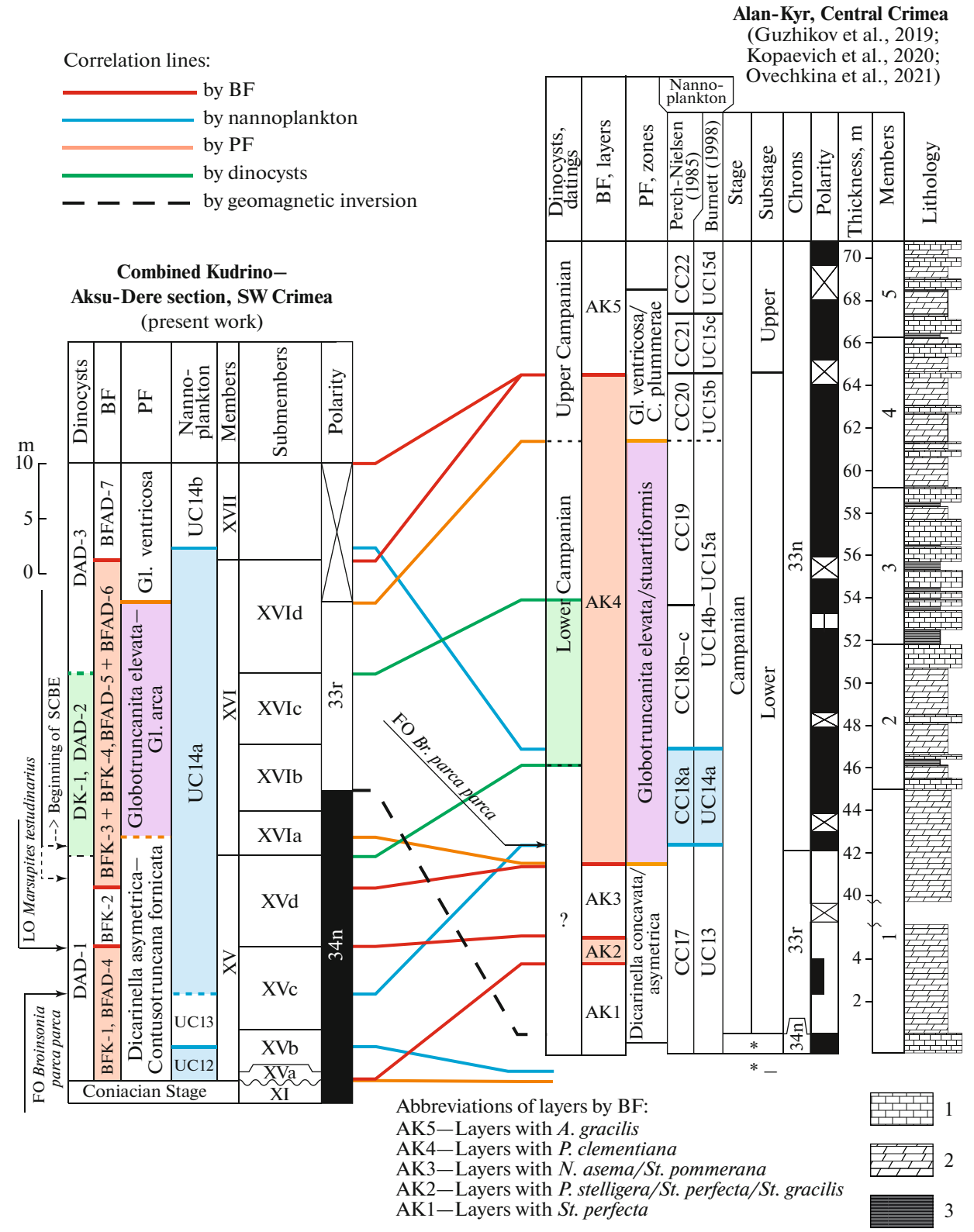

Fig. 7. Comparison of sections of the Santonian–Campanian boundary of Southwestern and Central Crimea. 1, Limestone; 2, marl; 3, calcareous clay.

assemblages (deep-water rocks of Central Crimea) and poorly representative micropaleontological data. The PF assemblage of the Alan-Kyr section is less diverse than that of the Kudrino-2 section, the nannoplankton is poorly or moderately preserved in both sections, and no dinocysts are found in some intervals of the sections.

In general, the results of biostratigraphic correlations do not correspond to magnetostratigraphic comparison of the sections. The consistent behavior of microfossil (except for BF) and paleomagnetic boundaries is observed only for the bases of the UC13 and Dicarinella asymetrica zones, which occur below the the base of the Chron 33r in various Crimean regions (Fig. 7). The correlation of younger rocks by nannoplankton and PF, however, cardinally contradicts the paleomagnetic data: the bases of the UC14 and Gl. elevata zones occur below the base of the Chron 33r in Southwestern Crimea and at its top in Central Crimea (Fig. 7). If we exclude the presence of a large hiatus in sedimentation at the Alan-Kyr section (which is baseless), then the results of the correlation indicate a temporal shift of micropaleontological boundaries comparable with the duration of the Chron 33r (~4 m.y.), which is absolutely unreal.

The lower Campanian Alan-Kyr rocks, in which we should expect reversed magnetization corresponding to the Chron 33r, could have been completely remagnetized by the later field of the opposite sign. This suggestion, however, is unsupported by a prefold age of components $\mathbf{J_n}$ corresponding to normal polarity (Guzhikov et al., 2019), which does not exclude possible remagnetization between the termination of lithification of sediments and folding.

Because of numerous contradictions in comparison of the Santonian–Campanian boundary of Southwestern and Central Crimea according to the data of various methods, neither micropaleontological nor paleomagnetic data on the Alan-Kyr section are perfect and none of the interpretation scenarios can unequivocally be accepted without additional detailed studies.

Possible Position of the Santonian–Campanian Boundary

Crinoids, ammonites, belemnites. The last occurrence (LO) of the index species *Marsupites testudinarius* was recommended as a main criterion of the Santonian–Campanian boundary (Gale et al., 2008; Hampton et al., 2007; Hancock et al., 1996; Ogg and Hinnov, 2012; Schulz et al., 1984). In the Aksu-Dere section, this bioevent was registered in the upper part of the Submember XVc. Thus, the Santonian–Campanian boundary (according to the occurrence of crinoids) should be determined by the top of the Submember XVc (Fig. 6). In the Kudrino-2 section, no findings of *M. testudinarius* are known.

The finding of *Parapuzosia* (*P.*) cf. *leptophylla* in the Aksu-Dere section (Baraboshkin and Fokin, 2019) confirms that the Submember XVc belongs to the Santonian. The *Actinocamax verus* and *A.* cf. *verus* belemnites (Baraboshkin and Fokin, 2019) do not determine the position of the Santonian–Campanian boundary, but also do not contradict the dating of the Member XVI as the early Campanian.

Calcareous nannoplankton. The results of determinations of nannoplankton in a narrow (1.5 m) Santonian–Campanian boundary interval (Fokin et al., 2018) admitted the position of the stage boundary near the top of the Member XV in the Aksu-Dere section. According to new data, the boundary of the UC13 and UC14 zones in the combined Kudrino–Aksu-Dere section is confined to the middle of the Submember XVc, and the base of the UC13 Zone occurs inside the Submember XVb (Fig. 6).

Judging from the proportions of the nannoplankton zones and stages (Fig. 8) accepted in the Geological Time Scale (GTS-2016) (Ogg et al., 2016), the lower boundary of the Campanian is located inside the Submember XVb, at least, at the level of Sample 21 or even below down the section. The comparison of these data with similar materials on other regions, however, shows ambiguous results. For example, the base of the UC13 Zone in the Seaford section (England) occurs in the middle Santonian; i.e., it is much more below the level of extinction of *Marsupites*, which marks the lower boundary of the Campanian (Thibault et al., 2016). In the Iranian Shahneshin section, the base of the UC14 Zone is also confined to the middle Santonian (Razmjooei et al., 2014, 2018) (Fig. 9). After the reinterpretation of stratigraphic data on the Shahneshin section (Razmjooei et al., 2020), the base of the UC14 Zone is combined with the lower boundary of the Campanian. Thus, the level of the Santonian–Campanian boundary in the combined Kudrino–Aksu-Dere section is located in the middle of the Submember XVc (Fig. 6).

Planktonic foraminifers. The identification of the Santonian–Campanian boundary in Crimea from the PF data meets some difficulties. The use of the Tethyan PF zonal scales in Peri-Tethyan Realm (Caron, 1985; Coccioni and Premoli Silva, 2015; Kopaevich, 2010; Kopaevich and Alekseev, 2019; Kopaevich and Vishnevskaya, 2016; Maslakova, 1967, 1978; Premoli Silva and Sliter, 1999; Robaszynski and Caron, 1995) is complicated by single specimens of PF index species. In Crimea, they are extremely rare or even absent such as, e.g., *Dicarinella concavata/asymetrica* (Maslakova, 1967, 1978). In these cases, we should use other taxa which are more geographically abundant such as *Contusotruncana fornicata* (Kopaevich, 2010; Kopaevich and Vishnevskaya, 2016; Vishnevskaya and Kopaevich, 2020; Walaszczyk and Peryt, 1998). Another reason is a mismatch of zonal boundaries with a stage boundary if it is accepted by the occur-

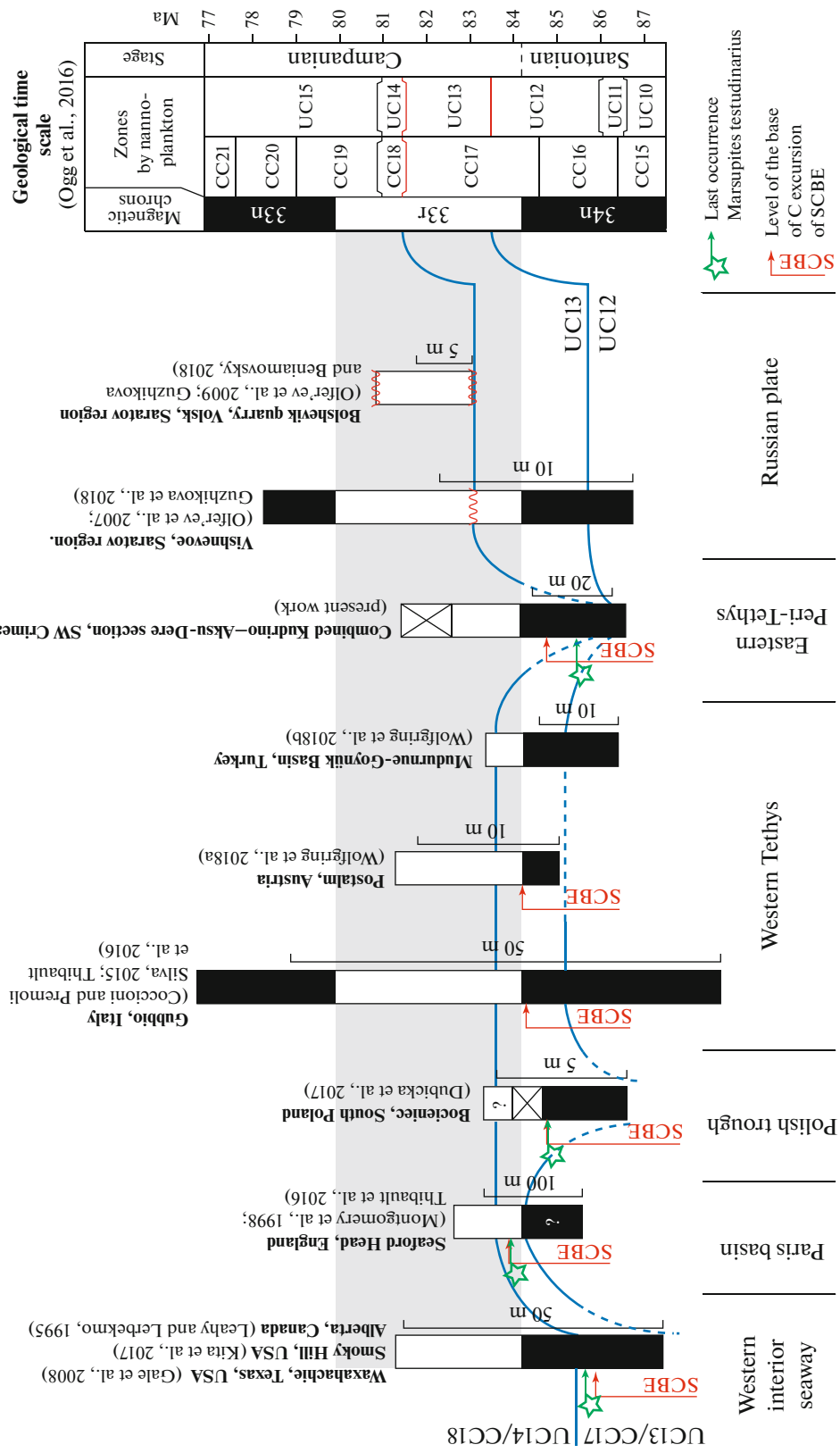

Fig. 8. Results of calibration of biostratigraphic boundaries (by nannoplankton and LO of *M. testuidinarius*) relative to inversion 34n–33r and SCBE.

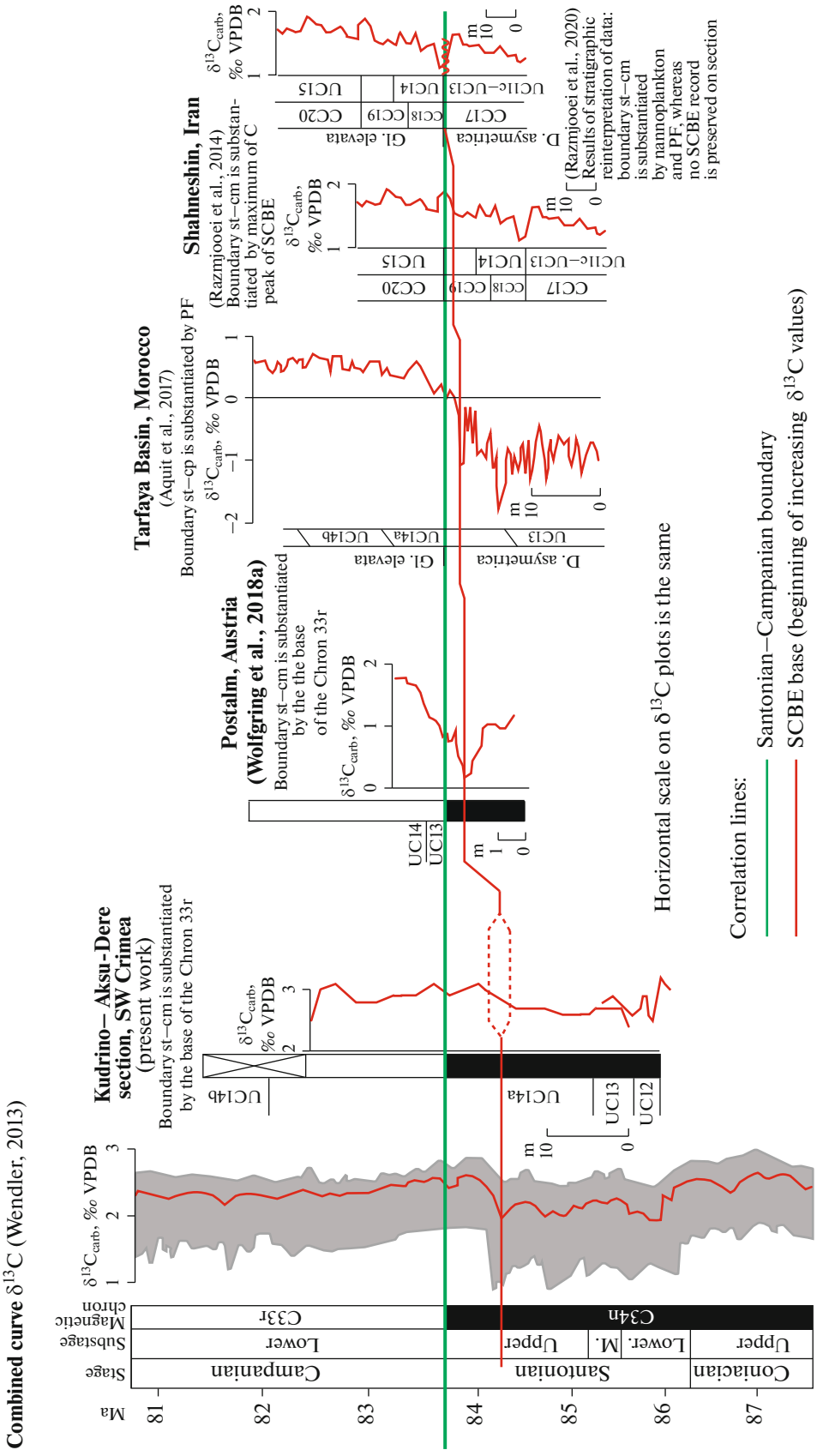

Fig. 9. The position of stratigraphic boundaries of various origins relative to the Santonian–Campanian boundary.

rence of *Marsupites*. The boundary criteria are also often ambiguous. The zones are reasonably named by species which are the most striking morphotypes characterizing precisely this stratigraphic range. At the beginning of their onset, however, they are rare and the first specimens are often indicated in the structure of PF associations of the previous zone. All this significantly complicates even the selection of the boundary between zones, as well as their correlation. In the Bottaccone section (Italy) (Premoli Silva and Sliter, 1995), the lower boundary of the Campanian corresponds to the LO of *Dicarinella concavata/asymetrica* at constant presence of *Globotruncanita elevata/stuartiformis*, the first specimens of which can occur in sediments of the previous zone. In the Kudrino-2 section, the boundary between stages (the base of the Gl. elevata Zone) follows this principle in the middle of the Submember XVIa (Fig. 6).

The Aksu-Dere section contains no index species and the zones are recognized on the basis of secondary features (i.e., onset of accompanying species). The Santonian–Campanian boundary in this section can follow the base of the Globotruncana arca Zone, which completely corresponds to the Gl. elevata Zone (Beniamovsky and Kopaevich, 2016; Bragina et al., 2016; Kopaevich et al., 2020; Maslakova, 1978) (Fig. 6).

Benthic foraminifers. Submembers XVb and XVc in the Aksu-Dere section contains a BF assemblage BFAD-4, which corresponds to the upper Santonian Pseudovalvulineria stelligera LC10a Subzone according to the scheme of Beniamovsky (2008), whereas the Member XVI corresponds to layers BFAD-5 and BFAD-6, which are compared with the lower Campanian Pseudogavelinella clementiana LC12 Zone according to the scheme of Maslakova, 1978; (2008). In addition, layers BFAD-5 contain both species *Bolivinoides strigillatus* (Chapman) and *Bolivinoides culverensis* (Barr), which allows comparison of these layers with the lower Campanian B. culverensis Zone (Walaszczyk et al., 2016). In spite of dating in scales for the European paleogeographic realm (Beniamovsky, 2008; Walaszczyk et al., 2016) and Southern England (Jenkins and Murray, 1989), the discussion on the early Campanian age of layers BFAD-5 and BFAD-6 in Crimea is premature, because the occurrence of *B. culverensis* (Barr) spans both the lower Campanian and terminal Santonian (Petters, 1977) and *Pseudogavelinella clementiana* (d'Orbigny) are found in marsupite layers (obviously Santonian) of Crimea (Maslakova, 1959). Thus, the range of layers BFAD-5 and BFAD-6 belongs to the Santonian–Campanian boundary, which is consistent with other data (except for nannoplankton).

In the Kudrino-2 section, the age of layers BFK-1 and BFK-2 is determined as the late Santonian; thus, the lower boundary of the Campanian in the combined section cannot occur below the middle part of the Submember XVd, which is in agreement with data on BF in the Aksu-Dere section. Layers BFK-3 and BFK-4 in the Kudrino-2 section correspond to layers BFAD-5 and BFAD-6 in the Aksu-Dere section; thus, the Santonian–Campanian boundary can occur in a range from the upper part of the Submember XVd to the top of the Member XVI (Fig. 6).

Dinocysts. The palynological data allow the position of the stage boundary in a range from the base of the Submember XVIa to the top of the Submember XVc, which is ascribed to the terminal part of the upper Santonian–the beginning of the Campanian on the basis of correlation with reference English sections (Fig. 6) (see section "Palynology" in (Guzhikov et al., 2021)).

Carbon isotopic stratigraphy. The comparison of C isotopic data of the Kudrino-2 section with a compilation $\delta^{13}C$ curve (Wendler, 2013) recognizes the SCBE (Santonian–Campanian Boundary Event). A strong increase in $\delta^{13}C$ values (the base of SCBE) of this section occurs slightly below the base of the Chron 33r, as well as on a global $\delta^{13}C$ curve (Fig. 9). The difference between the minimum and maximum values of $\delta^{13}C$ within the SCBE is almost the same (~0.7‰) in the Crimean section and on the averaged global $\delta^{13}C$ curve. The C chemostratigaphic data from various regions available after 2013 also record a positive C excursion near the Santonian–Campanian boundary (Wolfgring et al., 2018a). The $\delta^{13}C$ values of the Austrian Postalm section, as well as the Kudrino–Aksu-Dere section, start to increase slightly below the base of the Chron 33r (Figs. 8, 9). Additional evidence of valid C isotopic data of the combined Kudrino–Aksu-Dere section includes the higher $\delta^{13}C$ values of the underlying Coniacian rocks (Member XI), which correspond to the late Coniacian or/and middle Coniacian positive isotopic excursions (Fig. 9).

The SCBE isotopic excursion was suggested as one of markers of the Santonian–Campanian boundary (Gale et al., 1995, 2008), and according to this feature, the lower boundary of the Campanian in the Kudrino section occurs in the boundary interval of the Submembers XVd and XVIa (Fig. 6).

Sr isotopic stratigraphy. The Santonian–Campanian boundary on a global variation curve of the $^{87}Sr/^{86}Sr$ ratio of the Cretaceous ocean is confined to the changes of values from 0.70744–0.70748 to 0.70750–0.70751 (McArthur et al., 2012). Similar changes in $^{87}Sr/^{86}Sr$ values occur in the upper parts of the Submember XVb in the Aksu-Dere section (Fig. 5). The level of this isotopic transition is similar to the base of the nannoplankton UC13 Zone, but is located below the LO level of *Marsupites* confined to the top of the Submember XVc (Fig. 6). In the Kudrino-2 section, where Sr was studied only in the overlying rocks (Submembers XBc and XVd and Member XVI), all samples formally correspond to the Campanian $^{87}Sr/^{86}Sr$ values (0.70750–0.70755). This is slightly higher the values of typical Santonian seawater:

0.70740–0.70748 (McArthur et al., 2012).This difference (if the Sr isotopic system was undisturbed) can be interpreted as the Campanian age of the topmost part of the Submember XVb and the Member XVc or as partial isolation of the paleobasin during the accumulation of the late Santonian carbonate sediments. The latter scenario is unlikely, because, as is shown by example of the present-day Mediterranean intracontinental seas, the Sr isotopic composition is homogenized at a relatively high degree of isolation of basins and salinity of up to 10–18‰ (Kuznetsov et al., 2012). The discussion of problems of the age of sediments and the position of the stage boundary in the Kudrino–Aksu-Dere section on the basis of Sr isotopic data is hampered by inconsistency of studied samples to geochemical criteria. The comparison of our Sr isotopic composition with similar values in sediments of the same age from other regions (e.g., in the reference Santonian–Campanian sections in Austrian Alps) is difficult because of the absence of geochemical confirmation of preservation of Sr isotopic systems (Wagreich et al., 2010; Wolfgring et al., 2018a).

Magnetostratigraphy. The lower parts of the Kudrino–Aksu-Dere section (Member XV, Submember XVIa, and the lower part of the Submember XVIb) exhibit the normal polarity in contrast to the upper parts (upper two-thirds of Member XVIb, Submembers XVIc and XVId, and, probably, Member XVII). This is consistent with traditional ideas on the paleomagnetic structure of the Santonian–Campanian boundary reflected in the Geomagnetic Polarity Time Scale (GPTS) (Gradstein et al., 2020): according to these ideas, the topmost parts of the Chron 34n and the lowermost parts of the Chron 33r correspond to the Santonian and the beginning of the Campanian, respectively (Fig. 8). No commonly accepted viewpoint exists on the proportion between the lower boundaries of the Campanian Stage and the Chron 33r (because the GSSP of the Campanian is still undetermined). By analogy with the latest version of the GPTS (Gradstein et al., 2020), where the base of the Chron 33r coincides with the lower boundary of the Campanian, this stage boundary in the Kudrino-2 section is identified inside the Submember XVIb (the level between Samples 24 and 25) by the lower boundary of magnetozone R1 (Fig. 6).

Problems of Global Tracing of Stratigraphic Boundaries in the Santonian–Campanian Boundary and Selection of a Primary Marker of the Stage Boundary

Crinoids. The calibration of the LO of *Marsupites testudinarius* relative to geomagnetic reversal 34n–33r shows that it occurs above the reversal in the combined Santonian–Campanian section of Southern England, approximately at the level of reversal in the Polish Bocieniec section, and below the paleomagnetic boundary in Southwestern Crimea and North America (Fig. 8). The North American sections, however, contain *Marsupites* sp. in an assemblage with *Uintacrinus socialis* rather than *Marsupites testudinarius*. Judging from global synchronous reversal events, it can be concluded that *M. testudinarius* became extinct in England later than in other regions. Unfortunately, the American findings of *Marsupites* and paleomagnetic determinations originate from sections remote from each other, whereas the position of the base of the Chron 33r in the Bocieniec section can only be suggested, because the zone of reversed polarity is substantiated by anomalous paleomagnetic directions of only two levels. The exclusion of these unreliable data, however, does not affect the conclusions that the LO level of *M. testudinarius* in England is younger than in Crimea.

The diachronous LO of *M. testudinarius* is also identified relative the beginning of the positive C excursion of the SCBE. In the Kudrino–Aksu-Derev section, the SCBE-a and SCBE-b peaks cannot be recognized because of the limited amount of isotopic analyses. Thus, we conducted the chemostratigraphic correlation by a typical increase in $\delta^{13}C$ values, which registers the beginning the SCBE, rather than by C maxima as is accepted. In Seaford (England), Bocieniec (Poland), and Waxahachie (North Texas), the LO of *Marsupites* occurs ~2, ~0.5, and ~8 m above the level corresponding to the beginning of the SCBE, respectively, and 6 m below the isotopic marker in Southwestern Crimea (Fig. 6). Thus, the results of independent calibrations (by geomagnetic reversal and isotopic event) lead to a similar conclusion: *M. testudinarius* in Crimea became extinct earlier than in England.

In England, the LOs of marsupites and the beginning of the SCBE are younger than the geomagnetic reversal by ~450 k.y. (the period equivalent to the duration of the M. testudinarius Zone and part of the Uintacrinus socialis Zone or nannoplankton UC13ii Subzone) according to the results of astrochronological calibration of the Seaford section (Thibault et al., 2016).

In Texas, the time which lasted after the beginning of the isotopic event and before the extinction of marsupites is shorter than the duration of the nannoplankton UC13a Subzone (Gale et al., 2008) (~0.5 m.y., if we assume that the duration of all three subzones is approximately the same), i.e., a few hundred thousand years.

In the Kudrino–Aksu-Dere section, only part of the nannoplankton UC14a Subzone corresponds to the period from the extinction of *M. testudinarius* to the beginning of C excursion and geomagnetic reversal. If we orientate the GTS-2016 (Ogg et al., 2016), in which the duration of the UC14 Zone is ~200000 years, then the duration of each of the four nannoplankton subzones is no more than 50000 years. This estimate is the upper limit of the duration of a temporal shift between the LO of *M. testudinarius* and the beginning of the SCBE (or between the LO of *M. testudinarius* and geomagnetic reversal) in Crimea.

Our estimates of diachrony at global tracing of the LO of *Marsupites* are approximate. Nonetheless, they confirm doubts on reliable extinction as a marking event for the determination of the stratigraphic boundaries, which is reflected in rules of selection of the limitotype (*Dopolneniya...*, 2000; Remane et al., 1996). In any case, the limited area and rare occurrence of *M. testudinarius* are unavoidable disadvantages of the LO of this species as a main feature for the determination of the lower boundary of the Campanian (see section "Echinoderms" in (Guzhikov et al., 2021)).

Nannoplankton. The results of paleomagnetic calibration of the nannoplankton zones identified in the sections of various regions (Fig. 8), in our opinion, confirm the unsuitability of calcareous nannofossils as primary markers of the lower boundary of the Campanian Stage. It is noteworthy that the boundaries of zones can be isochronous within one paleobasin, e.g., Western Tethys. In other regions (e.g., from Western Interior Seaway to Tethys or from Western Tethys to Eastern Paratethys), the diachrony of the boundary of the UC13–UC14 (CC17–CC18) Zones relative to geomagnetic reversal is unambiguous (Fig. 8). The diachrony of the UC12–UC13 boundary is registered in comparison with GTS-2016 (Ogg et al., 2016); however, it is difficult to discuss this because of unclear calibration of a succession of zones by the nannoplankton with paleomagnetic scale. In spite of approved results of this calibration by a working group on Late Cretaceous fossils in London 2011 (Ogg and Hinnov, 2012), the situation is unclear.

The different age of the Boreal and Tethyan Zones by nannoplankton in the Santonian–Campanian boundary interval was independently identified from the results of a comprehensive study of the Shahneshin section in Iran and tracing the Santonian–Campanian boundary from Northwestern Europe to Zagros according to C isotopic data (Razmjooei et al., 2014). Our estimate of a temporal shift upon tracing boundaries of the nannoplankton zones in various paleobiogeographical provinces, as well as the estimates of Iranian colleagues, is several million years. Similar diachrony is inappropriate for the stratigraphy of the Santonian, which lasted ~2 m.y. (Gradstein et al., 2020). In spite of that, the stratification of the Shahneshin section is currently reconsidered in favor of the isochronous event of first occurrence (FO) of *Broinsonia parca parca*, which marks the base of the nannoplankton UC14 Zone (Razmjooei et al., 2020); the possibility of similar errors warns against selection of nannoplankton events as the main markers for global tracing of the Campanian lower boundary.

Planktonic foraminifers. According to the current ideas, the Santonian–Campanian boundary is close to the boundary between the Dicarinella asymetrica and Globotruncanita elevata Zones (Ogg et al., 2016). According to the paleomagnetic calibration (Fig. 10), the diachrony of the boundary between the D. asymetrica and Gl. elevata Zones is low relative to geomagnetic reversal. It is ubiquitously confined either to the topmost parts of the Chron 34n or to the lowermost parts of the Chron 33r, and in the Gubbio section, it almost coincides with the level of geomagnetic reversal (Fig. 10).

The use of the PF as one of main markers of the Santonian–Campanian boundary, however, is complicated in regions where the index species are either absent or rare. In the Upper Cretaceous Tuarkyr section (Turkmenistan), the Santonian–Campanian boundary confined to the middle part of the Chron 33r was established by L.F. Kopaevich by PF (Guzhikov et al., 2003), but no species *D. asymetrica* and *Gl. elevata* were found. According to the results of magnetochronological calibration, it can be concluded that the Campanian lower boundaries by PF in the North Mediterranean region and on the Turan Platform differ in time on the order of a few million years (Fig. 10). The PF assemblages in the Santonian–Campanian sections of the Russian Plate—the settlement of Vishnevoe (Guzhikova et al., 2018) and Bolshevik quarry in the town of Volsk (Guzhikova and Beniamovsky, 2018)—with paleomagnetic characteristics cannot be compared with the standard succession of the Tethyan Zones by PF (Fig. 10).

Thus, the PF can hardly be considered the main markers of the lower boundary of the Campanian globally. We meet this constantly, because the PF depend on the water parameters: temperature, depth, salinity, position relative to the coastline, etc. (Kopaevich and Gorbachik, 2017; Kopaevich and Vishnevskaya, 2016).

Benthic foraminifers. The benthic organisms depend more on the facies conditions than plankton; thus, the BF-based boundaries of stratigraphic units are expectedly diachronous relative to the reversal level in various regions (Fig. 11). The different position of the FO of *P. clementiana* (see above), to which the base of the lower Campanian eponymous zone is related, can be explained in various regions by migration of the species from the south. In Crimea, this species was identified in the Santonian marsupite layers (Maslakova, 1959), whereas, in the Russian Plate, it is a marker of the lower Campanian (Beniamovsky, 2008), which supports the invasion trend of *P. clementiana* to the northern latitudes from the south.

The BF-based correlation of zonal scales of various regions leads to the conclusions on the presence of a hiatus in the Kudrino-2 section equivalent by volume to one or several zones from BF schemes used in England, Poland, and the European part of Russia (Fig. 11). This is suspicious because the level of the possible hiatus occurs in the middle of the Submember XVd (Fig. 6) with no visible traces of hiatus. It is more likely that the use of BF-based zonal scales is effective only within certain paleobiogeographical provinces, whereas only some levels (e.g., the base of *P. clementiana*) can be traced in comparison of various paleobasins.

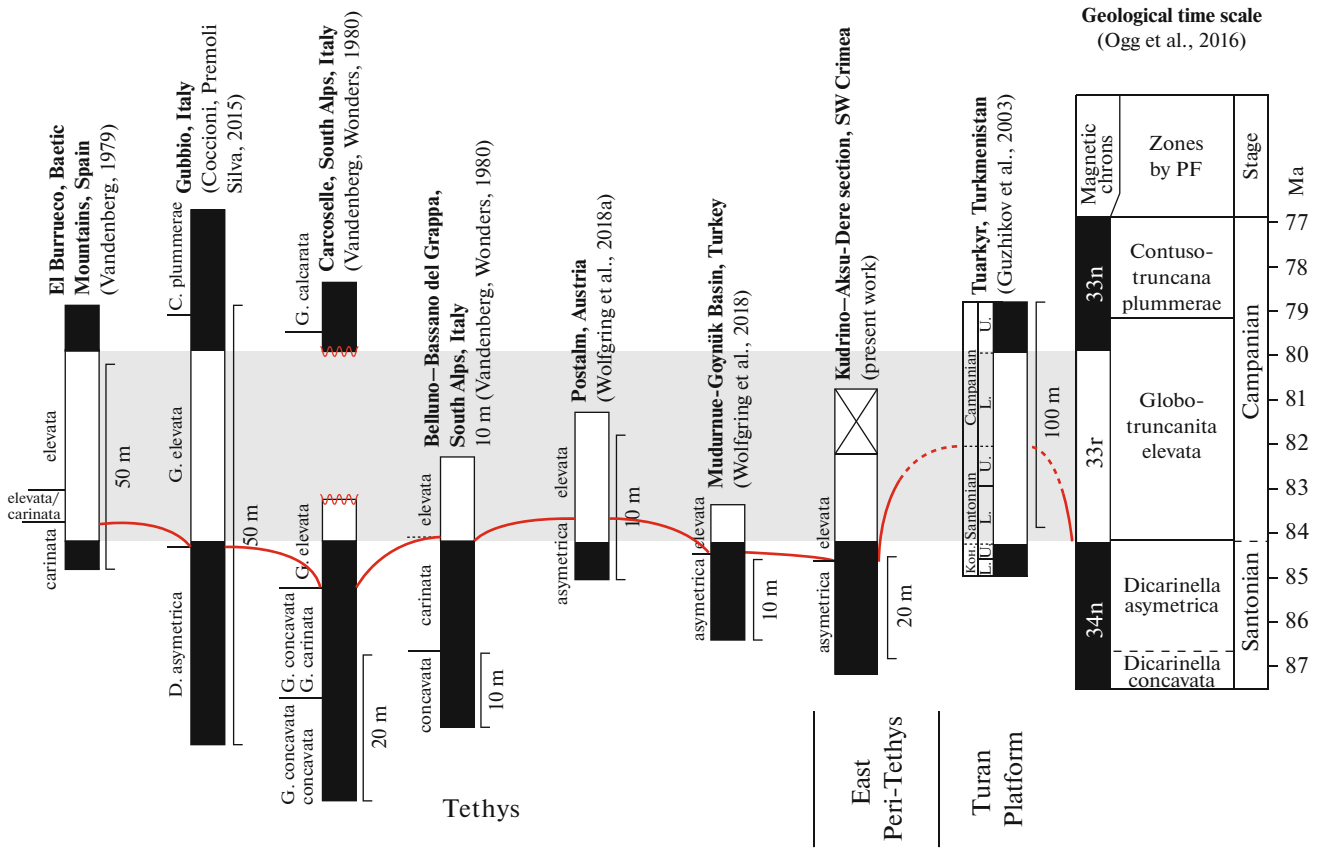

Fig. 10. Results of paleomagnetic calibration of biostratigraphic boundaries substantiated by planktonic foraminifers.

In general, the question of significant BF data for global correlations remains open and, at present, it is premature to consider BF as the leading markers of the Campanian lower boundary.

Dinocysts. The first detailed reports on the FO and LO of key dinocyst species in the Upper Cretaceous in different hemispheres of the Earth are given in (Foucher and Monteil, 1998; Williams et al., 2004). In contrast to nannoplankton and PF, there is no standard zonal scale on dinocysts, because their stratigraphic occurrence depends on the physicochemical characteristics of water masses, as well as the circulation of surface waters (Arai et al., 2000; Davies and Norris, 1980; Lebedeva, 2006; Lentin and Williams, 1980; Mudie, 1992; Norris, 1975; Williams et al., 1990, 2004); thus, the ranges of species are different in low, medium, and high latitudes.

In spite of significant progress in study of the Upper Cretaceous dinoflagellates (Aurisano, 1989; Davtalab et al., 2018; Ghasemi-Nejada et al., 2006; Pearce et al., 2020; Prince et al., 1999; Razmjooei et al., 2018), the results of detailed comprehensive stratigraphic studies of the associations of the Santonian–Campanian dinocysts together with orthostratigraphic fauna groups and isotopic and paleomagnetic data are few in number. One of the most complete works (Pearce et al., 2020) estimates the stratigraphic and paleogeographical distribution of key dinocyst species at the Santonian–Campanian boundary along with other bioevents and isotopic events. These authors confirmed the principles of the paleolatitudinal occurrence of dinocysts: many species are limited to the Northern Hemisphere or specific climate belts and only some of them are cosmopolite. Most interregional bioevents by dinocysts were identified in Northwestern Europe, which is generally explained by its more detailed study. Amid 13 dinocyst levels for the late Santonian–early Campanian, which are considered potential interregional stratigraphic markers, only the extinction of *Heterosphaeridium difficile* is almost global. Its age is 84.61 Ma (Pearce et al., 2020), which is close to the age of the beginning of the Campanian estimated at 83.7 ± 0.5 Ma in the latest version of the Geological Time Scale (GTS-2020) (Gradstein et al., 2020).

Chemo- and magnetostratigraphy. The isotopic–stratigraphic and paleomagnetic markers are globally isochronous; thus, they are used for the calibration of biostratigraphic boundaries in various regions. Theoretically, the chemo- and magnetostratigraphic characteristics can be acquired everywhere, but this is

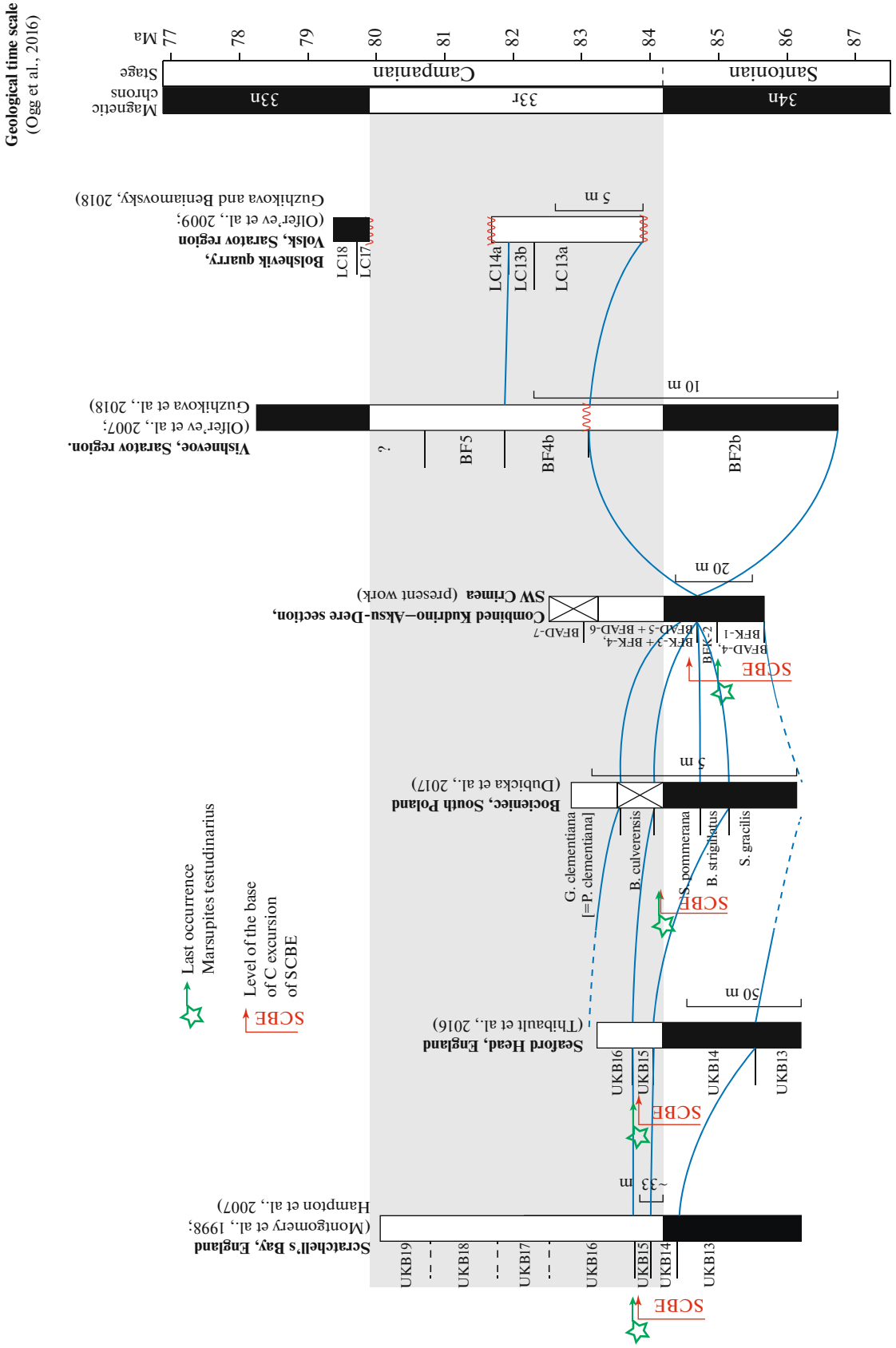

Fig. 11. Results of paleomagnetic calibration of biostratigraphic boundaries substantiated by benthic foraminifers.

hampered by various factors affecting the preservation of primary signals.

As was shown, the positions of the Campanian lower boundary determined by various methods not only do not coincide with each other in Southwestern Crimea, but even using the same method, they can be determined differently, because the tracing of the boundary depends on the selection of the scale or the reference section.

Similar differences are a result of diachrony of biostratigraphic boundaries. Thus, the isochronous correlation of the stratigraphic boundaries should enlist neopaleontological features. It is reasonable to use the base of the Chron 33r as a main criterion for the substantiation of the level of the Campanian lower boundary, which was proposed by the authors of the GTS (Gradstein et al., 2020; Ogg et al., 2016) and other researchers (Guzhikov et al., 2020; Wolfgring et al., 2018a, 2018b), as well as the positive C excursion of the SCBE.

We prefer the paleomagnetic criterion. The variations in stable isotopes of the Santonian–Campanian boundary of various regions, as seen from experience, can strongly differ. For example, the isotopic events (SCBE, MCE, LCE) cannot unambiguously be identified in Iran (Razmjooei et al., 2014, 2018, 2020), and the researchers of the Shakhneshin section relate these differences to possible features of evolution of the Zagros basin rather than to epigenetic changes and technical reasons (Razmjooei et al., 2020). The levels of geomagnetic inversion have absolute global isochrony.

The geomagnetic reversal as a marker of the lower boundary of the Campanian Stage is allowed by the rules of selection of the limitotype (*Dopolneniya...*, 2000). It is important to emphasize that the paleomagnetic feature is proposed for the substantiation of the level of the boundary rather than for the determination of the Santonian–Campanian boundary. The magnetostratigraphic method is unsuitable for dating of rocks and is effective only when coupled with paleontological and physicochemical data.

Combined Kudrino–Aksu-Dere Section: a Possible Candidate of the Limitotype of the Lower Boundary of the Campanian Stage

It is found as a result of paleontological, sedimentological, and physicochemical studies that the Santonian–Campanian boundary in the vicinity of the settlement of Kudrino is represented completely. The presence of hiatuses in sedimentation and condensation in the Submembers XVb–XVIa in the Aksu-Dere section is compensated by the absence of similar intervals in the Kurdino-2 section (Figs. 6, 12). Both sections exhibit no faults or strong diagenetic alteration.

The combined Kudrino–Aksu-Dere section contains diverse paleontological remains of macro- and microorganisms and includes carbonate facies which correspond to shelf open sea favorable for stratigraphic correlations. It registers most biotic events which are now considered the potential criteria of the lower boundary of the Campanian Stage (Fig. 12): (1) the LO level of crinoids *M. testudinarius*, (2) FO of B. *parca parca* (the base of the UC14/CC18 Zone by nannoplankton), and (3) LO of *D. concavata/asymetrica* at constant presence of *Gl. elevata/stuartiformis* (the base of the Gl. elevata Zone by PF).

The rocks are suitable for magneto- and chemostratigraphic study. The combined section has two magnetozones of normal and reversed polarity. The reversed polarity magnetozone is unambiguously identified as analog of the Chron 33r because of the absence of other chrons of reversed polarity near the Santonian–Campanian boundary interval.

No characteristic components of magnetization corresponding to reversed polarity have been distinguished yet, but it is possible that the increase in detailed sampling and repeated sampling of oriented specimens at a significant distance from the day surface will make it possible to obtain more reliable paleomagnetic characteristics of the section.

The variations in $\delta^{13}C$ values along the section register the SCBE in spite of the preliminary character of the data, which allows the future measurement of more detailed isotopic characteristics. Geomagnetic reversal 34n–33r and positive C excursion of the SCBE can be considered the main indicators of the Campanian lower boundary among abiotic events.

Thus, the combined Kudrino–Aksu-Dere section meets almost all requirements for the limitotype of the stage, including its location in an accessible region (Remane et al., 1996). The main candidates for the role of GSSP in North Texas and Southern England (stratigraphy.org) exceed the Crimean section by the detailed biostratigraphic characteristics, but this difference is not fundamental. It can be eliminated in the near future through more detailed and intense study, because the Santonian–Campanian boundary of Southwestern Crimea is comparable with age analogs of Texas and England by diversity of fossils. In spite of insufficient quality of paleomagnetic data in Crimea, the paleomagnetic characterization of the Santonian–Campanian of South England (Montgomery et al., 1998) is more problematic and its magnetostratigraphic interpretation is still a matter of debate (Razmjooei et al., 2014, 2018; Thibault et al., 2016). No paleomagnetic data on the Waxahachie section in Texas are available (Gale at al., 2008).

CONCLUSIONS

The main results of the comprehensive studies of the combined Kudrino–Aksu-Dere section are as follows.

(1) The paleontological and biostratigraphic characterization of the Santonian–Campanian boundary of Southwestern Crimea is significantly expanded. We

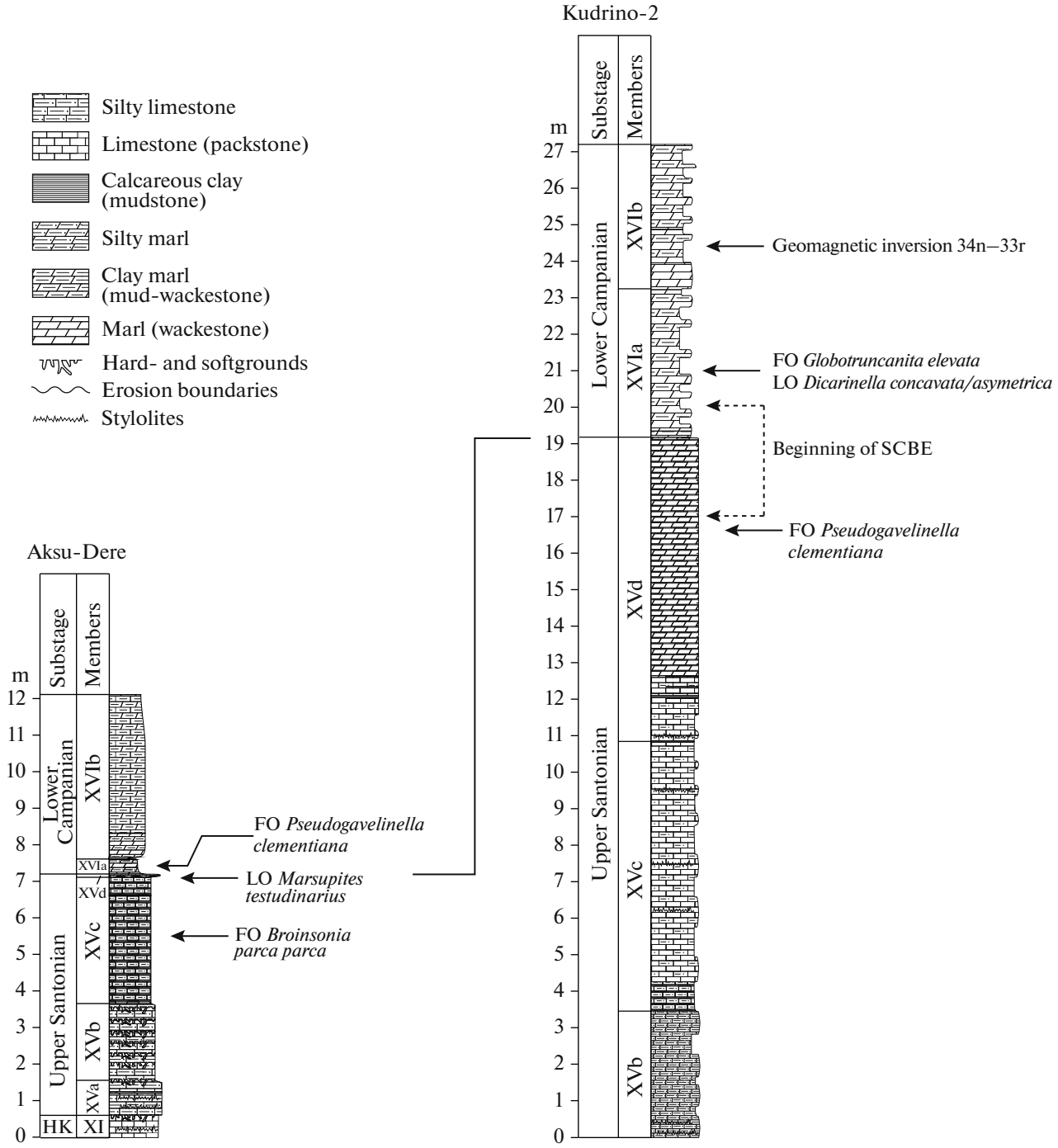

Fig. 12. Sequence of events in the Santonian–Campanian boundary of the Kudrino-2 and Aksu-Dere sections.

have identified the successions of zones by nannoplankton (UC12, UC13, and UC14 (subzones UC14a and UC14b)) and planktonic foraminifers (*C. fornicata*, *D. asymetrica*, *Gl. elevata–Gl. arca*, *Gl. ventricosa*) and the layers with assemblages of benthic foraminifers typical of the upper Santonian–lower Campanian of the Russian Plate and other regions. The palynological data are provided for the first time, as well as the identity of dinocyst assemblages in the studied rocks and in the boundary interval of the Santonian–Campanian of Western Europe.

The most important biotic events which mark the Santonian–Campanian boundary are recognized in the summarized section: LO of crinoids *Marsupites testudinarius*, FO of *B. parca parca* (the base of the UC14/CC18 Zone by nannoplankton), and LO of

D. concavata/asymetrica at constant presence of *Gl. elevata/stuartiformis* (the base of the Gl. elevata Zone by PF).

(2) The paleomagnetic characteristics and data on stable C, O, and Sr isotopes are provided for the Santonian and lower Campanian rocks of Southwestern Crimea for the first time. The magnetozones of normal and reversed polarity (analogs of chrons 34n and 33r) are identified. The level of geomagnetic inversion 34n–33r in the combined Kudrino–Aksu-Dere section is located slightly higher than the LO of *M. testudinarius*, but it is close to the position of the lower boundary of the Campanian, which is identified by PF.

The positive shift of $\delta^{13}C$ values (up to 0.7‰), which supposedly corresponds to the SCBE, is confined to the Santonian–Campanian boundary substantiated by foraminifers and dinocysts.

The Sr isotopic characteristic shows the increase in the $^{87}Sr/^{86}Sr$ ratio up the section from 0.70741–0.70748 to 0.70750–0.70753, which is similar to the change marking the Santonian–Campanian boundary on the global curve of $^{87}Sr/^{86}Sr$ variations (McArthur et al., 2012). This isotopic transition occurs stratigraphically below the LO of *M. testudinarius*, which is suggested as a main feature for the determination of the lower boundary of the Campanian, and the onset of typically Campanian foraminiferal assemblages. The discussion on different identification of the position of the stage boundary, which is determined from Sr stratigraphy and other methods, however, is premature because of possible disturbance of Sr isotopic systems of the studied samples owing to interaction of rocks with surface waters. It is not excluded that more reliable estimates of the $^{87}Sr/^{86}Sr$ ratio will be typical of samples collected at a significant distance from the surface or of belemnites and other fossils, which are most suitable for the estimates of the Sr isotopic composition of seawater (Jones et al., 1994; Kuznetsov et al., 2017, 2018).

(3) The paleomagnetic reference levels are calibrated against the levels of geomagnetic reversal 34n–33r and isotopic SCBE. It is shown that the temporal shift of stratigraphic boundaries substantiated by nannoplankton can be on the order of 10^6 years in remote regions.

(4) The boundary Santonian–Campanian isotopic event SCBE on the territory of Southwestern Crimea was caused by evolved transgression, which followed the drop in sea level and cooling of waters. The positive $\delta^{13}C$ peak almost coincides with appearance of regular pyroclastic admixture in the section, which was related to the activation of volcanism along the Middle Mountain–Pontides–Transcaucasian region (Nikishin et al., 2013) at the Santonian–Campanian boundary.

(5) The Kudrino–Aksu-Dere section is comparable with GSSP candidates of the Campanian lower boundary in North Texas and Southern England by the completeness of the boundary interval of the Santonian–Campanian, diversity of paleontological remains, suitable rocks for magneto- and chemostratigraphic study, and accessible position. Therefore, it can also be a potential candidate for the limitotype or auxiliary section of the lower boundary of the Campanian Stage.

The presentation of the Kudrino–Aksu-Dere section as a GSSP to the International Commission on Stratigraphy requires continuation of its comprehensive studies. Our preliminary results indicate that, by a series of parameters, the Crimean section after the detailed studies will exceed American and British analogs from the viewpoint of requirements for the selection of the global stratotype point. The search for more exposed and complete sections should also be continued in the Kacha–Belbek interfluve.

ACKNOWLEDGMENTS

We are grateful to A.G. Manikin, V.A. Grishchenko, and E.V. Naumov (Saratov State University) and D.S. Bolotova (Moscow State University) for the participation in field study of the section; V.E. Pavlov, R.V. Veselovskii, G.P. Markov, and other colleagues from the Laboratory of Main Geomagnetic Field and Rock Magnetism of the IPE RAS for the possibility of measurements on a cryogenic magnetometer; D.K. Nurgaliev and D.M. Kuzina (Kazan Federal University) and A.M. Surinskii (Saratov State University) for help in work with coercivity spectrometer; O.V. Volina (Chemical Analysis and Materials Research Center, St. Petersburg State University) for atomic emission analysis; and I.V. Smoleva (Center for Collective Use Geonauka, Institute of Geology, Komi Research Center, Ural Branch, Russian Academy of Sciences) for stable isotope analysis.

FUNDING

This work was supported by the Russian Foundation for Basic Research, project no. 18-05-00784-a. The results of studies of planktonic foraminifers were supported by the Russian Foundation for Basic Research, project no. 18-05-00-503-a. The determinations of benthic foraminifers were conducted by I.P. Ryabov and supported by the Russian Science Foundation, project no. 20-77-00028. The study of ichnofossils and determination of cephalopods were conducted by E.Yu. Baraboshkin within the framework of state contract no. AAAA-A16-116033010096-8 (Moscow State University).

Reviewers A.Yu. Kazanskii, B.G. Pokrovskii, and V.S. Vishnevskaya

REFERENCES

AGICO (Advanced Geoscience Instruments Company). www.agico.com/text/software/anisoft/anisoft.php

Aquit, M., Kuhnt, W., Holbourn, A., Chellai, E.H., Lees, J.A., Kluth, O., and Jabour, H., Complete archive of late Turo-

nian to early Campanian sedimentary deposition in newly drilled cores from the Tarfaya Basin, SW Morocco, *Bull. Geol. Soc. Am.*, 2017, vol. 129, pp. 137–151.

Arai, M., Neto, J.B., Lana, C.C., and Pedrão, E., Cretaceous dinoflagellate provincialism in Brazilian marginal basins, *Cretaceous Res.*, 2000, vol. 21, nos. 2–3, pp. 351–366.

Aurisano, R.W., Upper cretaceous dinoflagellate biostratigraphy of the subsurface Atlantic coastal plain of New Jersey and Delaware, U.S.A., *Palynology*, 1989, vol. 13, no. 1, pp. 143–179.
https://doi.org/10.1080/01916122.1989.9989359

Baraboshkin, E.Yu. and Fokin, P.A., Cephalopods from Santonian/Campanian (Upper Cretaceous) boundary interval of the Aksudere section (Crimean Mountains), *Byull. Mosk. O-va Ispyt. Prir., Otd. Geol.*, 2019, vol. 94, pp. 77–84.

Baraboshkin, E.Yu., Guzhikov, A.Yu., Aleksandrova, G.N., Fomin, V.A., Pokrovsky, B.G., Grishchenko, V.A., Manikin, A.G., and Naumov, E.V., New sedimentological, magnetostratigraphic, and palynological data on the Campanian–Maastrichtian section of Beshkosh Mountain, South-Western Crimea, *Stratigr. Geol. Correl.*, 2020, vol. 28, no. 6, pp. 816–858.

Beniamovsky, V.N., Infrazonal biostratigraphy of the Upper Cretaceous in the East European Province based on benthic foraminifers, Part 1: Cenomanian and Coniacian, *Stratigr. Geol. Correl.*, 2008a, vol. 16, no. 3, pp. 257–266.

Beniamovsky, V.N. and Kopaevich, L.F., The Alan-Kyr Coniacian–Campanian section (Crimean Mountains): Biostratigraphy and paleobiogeography aspects, *Moscow Univ. Geol. Bull.*, 2016, vol. 71, no. 3, pp. 217–233.

Besse, J. and Courtillot, V., Apparent and true polar wander and the geometry of the geomagnetic field over the last 200 Myr, *J. Geophys. Res.*, 2002, vol. 107, no. 11, pp. 1–31.

Bragina, L.G., Beniamovsky, V.N., and Kopaevich, L.F., Radiolarians, foraminifers, and biostratigraphy of the Coniacian–Campanian deposits of the Alan-Kyr section, Crimean Mountains, *Stratigr. Geol. Correl.*, 2016, vol. 24, no. 1, pp. 39–57.

Burov, B.V. and Yasonov, P.G., *Vvedenie v differentsial'nyi termomagnitnyi analiz gornykh porod* (Introduction to the Differential Thermomagnetic Analysis of Rocks), Kazan: Kazan. Gos. Univ., 1979 [in Russian].

Caron, M., Cretaceous planktic foraminifera, in *Plankton Stratigraphy*, Bolli, H.M., Saunders, J., and Persh-Nielsen, K., Eds., Cambridge: Univ. Press, 1985, pp. 17–86.

Chadima, M. and Hrouda, F., Remasoft 3.0 a user-friendly paleomagnetic data browser and analyzer, *Travaux Géophysiques*, 2006, vol. XXVII, pp. 20–21.

Coccioni, R. and Premoli Silva, I., Revised Upper Albian–Maastrichtian planktonic foraminiferal biostratigraphy and magnetostratigraphy of the classical Tethyan Gubbio section (Italy), *Newsl. Stratigr.*, 2015, vol. 48, pp. 47–90.

Davies, E.H. and Norris, G., Latitudinal variations in encystment modes and species diversity in jurassic dinoflagellates, in *The Continental Crust and its Mineral Deposits*, Strangway, D.W., Ed., *Geol. Assoc. Can. Spec. Pap.*, 1980, vol. 20, pp. 361–373.

Davtalab, E., Vahidinia, M., Ghasemi-Nejad, E., and Ashouri, A., Planktonic foraminifera and dinoflagellate cysts, Upper Cretaceous Abderaz Formation, Koppeh-Dagh Basin, NE Iran, *Stratigraphy*, 2018, vol. 15, no. 1, pp. 47–66.
https://doi.org/10.29041/strat.15.1.47-66

Dopolneniya k Stratigraficheskomu kodeksu Rossii (Supplements to the Stratigraphic Code of Russia), St. Petersburg: Vseross. Nauchno-Issled. Geol. Inst., 2000 [in Russian].

Dubicka, Z., Jurkowska, A., Thibault, N., Razmjooei, M.J., Wójcik, K., Gorzelak, K., and Felisiak, I., An integrated stratigraphic study across the Santonian/Campanian boundary at Bocieniec, southern Poland: a new boundary stratotype candidate, *Cretaceous Res.*, 2017, vol. 20, pp. 61–85.

Dunlop, D., Theory and application of the Day plot (Mrs/Ms versus Hcr/Hc) 1. Theoretical curves and tests using titanomagnetite data, *J. Geophys. Res.*, 2056, vol. 107, no. B3.
https://doi.org/10.1029/2001JB000487

Fokin, P.A., Kopaevich, L.F., Ustinova, M.A., and Kosorukov, V.L., The Santonian–Campanian deposits in the Aksudere section (Crimea, Bakhchisaray area), in *Melovaya sistema Rossii i blizhnego zarubezh'ya: problemy stratigrafii i paleogeografii. Mater. IX Vseross. soveshch., Belgorod, 17-21 sentyabrya 2018 g* (Proc. IX All-Russ. Conf. "Cretaceous System of Russia and CIS Countries: Problems of Stratigraphy and Paleogeography," Belgorod, September 17–21, 2018), Baraboshkin, E.Yu., Ed., Belgorod: POLITERRA, 2018, pp. 278–282.

Foucher, J.-C. and Monteil, E., Dinoflagellate cysts, in *Mesozoic and Cenozoic Sequence Stratigraphy of European Basins*, de Graciansky P.-C., Hardenbol, J., Jacquin, T., and Vail, P.R., Eds., *SEPM Spec. Publ.*, 1998, no. 60.

Gale, A.S., Montgomery, P., Kennedy, W.J., Hancock, J.M., Burnett, J.A., and McArthur, J.M., Definition and global correlation of the Santonian–Campanian Boundary, *Terra Nova*, 1995, no. 7, pp. 611–622.

Gale, A.S., Hancock, J.M., Kennedy, J.W., Petrizzo, M.R., Lees, J., Walaszczyk, I., and Wray, D., An integrated study (geochemistry, stable oxygen and carbon isotopes, nannofossils, planktonic foraminifera, inoceramid bivalves, ammonites and crinoids) of the Waxahachie Dam Spillway section, north Texas: A possible boundary stratotype for the base of the Campanian Stage, *Cretaceous Res.*, 2008, vol. 29, no. 1, pp. 131–167.

Ghasemi-Nejada, E., Hobbi, M.H., and Schiøler, P., Dinoflagellate and foraminiferal biostratigraphy of the Gurpi Formation (upper Santonian–upper Maastrichtian), Zagros Mountains, Iran, *Cretaceous Res.*, 2006, vol. 27, no. 6, pp. 828–835.

Gradstein, F.M., Ogg, J.G., Schmitz, M.B., and Ogg, G.M., *Geologic Time Scale 2020. Vol. 2*, Amsterdam, Oxford, Cambridge: Elsevier, 2020.

Guzhikov, A.Yu., Solving unsolvable problems in stratigraphy (Comments to the paper "New data on the magnetostratigraphy of the Jurassic–Cretaceous boundary interval, Nordvik Peninsula (northern East Siberia)" by V.Yu. Bragin, O.S. Dzyuba, A.Yu. Kazansky, and B.N. Shurygin), *Russ. Geol. Geophys.*, 2013, vol. 54, no. 3, pp. 349–354.

Guzhikov, A.Yu. and Feduleev, D.V., Paleomagnetism of Coniacian–Santonian deposits of SW Crimea, in *Mater. XXV yubileinoi Vseross. shkoly-seminara po problemam paleomagnetizma i magnetizma gornykh porod (s mezhdunarodnym uchastiem)*, Moskva–Borok, 25–29 sentyabrya 2019 g (Proc. XXV Jubilee All-Russ. School-Sem. (with Int. Particpation) on Problems of Rock Paleomagnetism and Mag-

netism), Shcherbakov, V.P., Ed., Moscow–Yaroslavl: Filigran', 2019, pp.103–108.

Guzhikov, A.Yu., Molostovskii, E.A., Nazarov, Kh., Fomin, V.A., Baraboshkin, E.Yu., and Kopaevich, L.F., Magnetostratigraphic data on the Upper Cretaceous of Tuarkyr. (Turkmenistan) and their implications for the general paleomagnetic time scale, *Izv., Phys. Solid Earth*, 2003, vol. 39, no. 9, pp. 728–740.

Guzhikov, A.Yu., Aleksandrova, G.N., and Baraboshkin, E.Yu., New sedimentological, magnetostratigraphic, and palynological data on the Upper Cretaceous Alan-Kyr Section (Central Crimea), *Moscow Univ. Geol. Bull.*, 2020a, vol. 75, no. 1, pp. 20–30.

Guzhikov A.Yu., Aleksandrova, G.N., Baraboshkin, E.Yu., Ryabov, I.P., and Ustinova, M.A., New data on bio- and magnetostratigraphy of the Santonian–Campanian boundary interval (SW Crimea), in *Mater. X Vseross. Soveshch "Melovaya sistema Rossii i blizhnego zarubezh'ya: problemy stratigrafii i paleogeografii". Magadan, 20-25 sentyabrya 2020 g* (Proc. X All-Russ. Conf. "Cretaceous System of Russia and CIS Countries: Problems of Stratigraphy and Paleogeography," Magadan, September 20–25, 2020), Baraboshkin, E.Yu. and Guzhikov, A.Yu., Eds., Magadan: OAO "MAOBTI", 2020b, pp. 76–80.

Guzhikov, A.Yu., Baraboshkin, E.Yu., Aleksandrova, G.N., Ryabov, I.P., Ustinova, M.A., Kopaevich, L.F., Mirantsev, G.V., Kuznetsov, A.B., Fokin, P.A., and Kosorukov, V.L., Bio-, chemo-, and magnetostratigraphy of the Santonian–Campanian boundary in the Kudrino and Aksu-Dere sections, (SW Crimea): Problems of global correlation and selection of the lower boundary stratotype of the Campanian. Paper 1. Geological framework, sedimentology, biostratigraphy, *Stratigr. Geol. Correl.*, 2021, vol. 29, no. 4, pp. 71–117.

Guzhikova, A.A., The first magnetostratigraphic data on the Maastrichtian of the Crimean Mountains (Bakhchisaray Region), *Izv. Saratov. Univ. Nov. Ser. Ser. Nauki o Zemle*, 2019, vol. 18, no. 1, pp. 41–49.

Guzhikova, A.A. and Beniamovsky, V.N., The Campanian–Maastrichtian magnetostratigraphy of the Volga region (vicinity of Volsk town), *Russ. Geol. Geophys.*, 2018, vol. 59, no. 3, pp. 276–284.

Guzhikova, A.A., Guzhikov, A.Yu., Grishchenko, V.A., and Manikin, A.G., The Upper Cretaceous magnetostratigraphy of the Lower Volga Region, in *Mater. 12-i Mezhd. shkoly-konf. "Problemy geokosmosa". Sankt-Peterburg, Petergof, 8–12 oktyabrya 2018 g* (Proc. 12th Int. School-Conf. "Problems of Geospace". St. Petersburg, Peterhof, October 8–12, 2018), Bobrov, N.Yu., Zolotova, N.V., Kosterov, A.A., and Yanovskaya, T.B., Eds., St. Petersburg: Izd. VVM, 2018, pp. 78–83.

Hampton, M.J., Bailey, H.W., Gallagher, L.T., Mortimore, R.N., and Wood, C.J., The biostratigraphy of Seaford Head, Sussex, southern England; an international reference section for the basal boundaries for the Santonian and Campanian Stages in chalk facies, *Cretaceous Res.*, 2007, vol. 28, pp. 46–60.

Hancock, J.M., Gale, A.S., Gardin, S., Kennedy, W.J., Lamolda, M.A., Matsumoto, T.M., and Naidin, D.P., The Campanian Stage, in *Proc. Second Int. Symp. on Cretaceous Stage Boundaries*, Rawson, P.F., Dhondt, J.M., Hancock, J.M., and Kennedy, W.J., Eds., *Bull. Inst. R. Sci. Nat. Belg., Sci. Terre,* 1996, vol. 66 (Suppl.), pp. 103–109.

Jackson, M. and Bowles, J.A., Curie temperatures of titanomagnetite in ignimbrites: effects of emplacement temperatures, cooling rates, exsolution, and cation ordering, *Geochem. Geophys. Geosyst.*, 2014, vol. 15, pp. 4343–4368.

Jones, C.E., Jenkyns, H.C., Coe, A.L., and Hesselbo, S.P., Strontium isotopes in Jurassic and Cretaceous seawater, *Geochim. Cosmochim. Acta*, 1994, vol. 58, no. 14, pp. 3061–3074.

Kita, Z.A., Watkins, D.K., and Sageman, B.B., High-resolution calcareous nannofossil biostratigraphy of the Santonian/Campanian Stage boundary, Western Interior Basin, USA, *Cretaceous Res.*, 2017, vol. 69, pp. 49–55.

Kopaevich, L. F., Upper Cretaceous zonal scheme for Crimea–Caucasus area based on globotruncanids (planktonic foraminifers), *Byull. Mosk. O–va Ispyt. Prir., Otd. Geol.,* 2010, vol. 85, no. 5, pp. 40–52.

Kopaevich, L.F. and Alekseev, A.S., Nina Ivanovna Maslakova and the development of the Upper Cretaceous zonal scheme for South Europe based on plankrtonic formanifers, *Byull. Mosk. O–va Ispyt. Prir., Otd. Geol.,* 2019, vol. 94, pp. 3–13.

Kopaevich, L.F. and Gorbachik, T.N., Shell morphology in Cretaceous planktonic foraminifers as a means for modeling paleoenvironments, *Paleontol. J.*, 2017, no. 1, pp. 3–15.

Kopaevich, L.F. and Vishnevskaya, V.S., Cenomanian–Campanian (Late Cretaceous) planktonic assemblages of the Crimea-Caucasus area: Palaeoceanography, palaeoclimate and sea level changes, *Palaeogeogr., Palaeoclimatol., Palaeoecol.*, 2016a, vol. 441, Spec. Iss., pp. 493–515. https://doi.org/10.1016/j.palaeo.2015.09.024

Kopaevich, L.F. and Vishnevskaya, V.S., Distribution of water masses and dynamics of paleogeography in the Crimea–North Caucasus Region in the Late Cretaceous, in *Paleontologiya. Stratigrafiya. Astrobiologiya. K 80-letiyu A.Yu. Rozanova* (Paleontology. Stratigraphy. Astrobiology. To the 80th Anniversary of A.Yu. Rozanov), Moscow: Paleontol. Inst. Ross. Akad. Nauk, 2016b, pp. 243–256.

Kopaevich, L.F., Proshina, P.A., Ryabov, I.P., Ovechkina, M.N., and Grechikhina, N.O., New microfossils data about the Santonian-Campanian boundary in the Alan-Kyr section (Central Crimea), *Moscow Univ. Geol. Bull.*, 2020, no. 2, pp. 43–50.

Kuznetsov, A.B., Ovchinnikova, G.V., Krupenin, M.T., Gorokhov, I.M., Maslov, A.V., Kaurova, O.K., and Ellmies, R., Diagenesis of carbonate and sideritre deposits of the Lower Riphean Bakal Formation, the Southern Urals: Sr isotopic characteristics and Pb–Pb age, *Lithol. Miner. Resour.*, 2005, no. 3, pp. 195–215.

Kuznetsov, A.B., Semikhatov, M.A., Maslov, A.V., Gorokhov, I.M., Prasolov, E.M., Krupenin, M.T., and Kislova, I.V., New data on Sr-and C-isotopic chemostratigraphy of the Upper Riphean type section (Southern Urals), *Stratigr. Geol. Correl.*, 2006, vol. 14, no. 6, pp. 602–628.

Kuznetsov, A.B., Semikhatov, M.A., and Gorokhov, I.M., The Sr isotope composition of the world ocean, marginal and inland seas: Implications for the Sr isotope stratigraphy, *Stratigr. Geol. Correl.*, 2012, vol. 20, no. 6, pp. 501–515.

Kuznetsov, A.B., Izokh, O.P., Dzyuba, O.S., and Shurygin, B.N., Sr isotope composition in belemnites from the Jurassic–Cretaceous boundary section (Maurynya River, Western Siberia), *Dokl. Earth Sci.*, 2017, vol. 477, no. 2, pp. 1408–1413.

Kuznetsov, A.B., Semikhatov, M.A., and Gorokhov, I.M., Strontium isotope stratigraphy: Principles and state of art, *Stratigr. Geol. Correl.*, 2018, vol. 26, no. 4, pp. 367–386.

Leahy, G.D. and Lerbekmo, J.F., Macrofossil magnetobiostratigraphy for the upper Santonian–lower Campanian interval in the Western Interior of North America: comparisons with European stage boundaries and planktonic foraminiferal zonal boundaries, *Can. J. Earth Sci.*, 1995, vol. 32, pp. 247–260.

Lebedeva, N.K., *Dinocyst biostratigraphy of the Upper Cretaceous of northern Siberia*, Doctoral (Geol.-Mineral.) Dissertation, Novosibirsk: Inst. Geol. Nefti Gaza Sib. Otd. Ross. Akad. Nauk, 2006.

Lentin, J.K. and Williams, G.L., Dinoflagellate provincialism with emphasis on Campanian peridiniaceans, *Am. Assoc. Stratigr. Palynol. Contrib. Ser.*, 1980, vol. 7, pp. 1–47.

Maslakova, N.I., The Crimea, in *Atlas verkhnemelovoi fauny Severnogo Kavkaza i Kryma* (Atlas of Upper Cretaceous Fauna of Northern Caucasus and Crimea), Moskvina, M.M., Ed., Moscow: Gostoptekhizdat, 1959, pp. 60–84.

Maslakova, N.I., *Globotrunkanides and their significance for the Upper Cretaceous stratigraphy of Crimea, Caucasus, and Soviet Carpathians*, Doctoral (Geol.-Mineral.) Dissertation, Moscow: Mosk. Gos. Univ., 1967.

Maslakova, N.I., *Globotrunkanidy yuga evropeiskoi chasti SSSR* (Globotrunkanides of the South of the European Part of the USSR), Moscow: Nauka, 1978 [in Russian].

McArthur, J.M., Howarth, R.J., and Shields, G.A., Strontium isotope stratigraphy, in *The Geologic Time Scale 2012*, Gradstein, F.M., Ogg, J.G., Schmitz, M.D., and Ogg, G.M., Eds., Amsterdam: Elsevier, 2012, vol. 1, pp. 127–144.

Mikhailov, G.G. Leonovich, B.I., and Kuznetsov, Yu.S., *Termodinamika metallurgicheskikh protsessov i system* (Thermodynamics of Metallurgical Processes and Systems), Moscow: ID MISiS, 2009 [in Russian].

Molostovskii, E.A. and Khramov, A.N., *Magnitostratigrafiya i ee znachenie v geologii* (Magnetostratigraphy and its Significance for Geology), Saratov: Saratov. Gos. Univ., 1997 [in Russian].

Montgomery, P., Hailwood, E.A., Gale, A.S., and Burnett, J.A., The magnetostratigraphy of Coniacian–Late Campanian chalk sequences in southern England, *Earth Planet. Sci. Lett.*, 1998, vol. 156, pp. 209–224.

Mudie, P.J., Circum-Arctic Quaternary and Neogene marine palynofloras: Paleoecology and statistical analysis, in *Neogene and Quaternary Dinoflagellates Cysts and Acritarchs*, Head, M.J., and Wrenn, J.H., Eds., Dallas: Am. Assoc. Stratigr. Palynol. Found., 1992, pp. 347–390.

Nikishin, A.M., Khotylev, A.O., Bychkov, A.Yu., Kopaevich, L.F., Petrov, E.I., and Yapaskurt, V.O., Cretaceous volcanic belts and the evolution of the Black Sea Basin, *Moscow Univ. Geol. Bull.*, 2013, no. 2, pp. 141–154.

Norris, G., Provincialism of Callovian–Neocomian dinoflagellate cysts in the northern and southern hemispheres, *Am. Assoc. Stratigr. Palynol. Contrib. Ser.*, 1975, vol. 4, pp. 29–35.

Ogg, J.G. and Hinnov, L.A., Cretaceous, in *The Geologic Time Scale*, Gradstein, F.M., Ogg, J.G., Schmitz, M.D., and Ogg, G.M., Eds., Amsterdam: Elsevier, 2012, pp. 793–855.

Ogg, J.G., Ogg, G.M., and Gradstein, F.M., *A Concise Geologic Time Scale*, New York: Elsevier, 2016.

Olfer'ev, A.G., Beniamovsky, V.N., Vishnevskaya, V.S., Ivanov, A.V., Kopaevich, L.F., Pervushov, E.M., Sel'tser, V.B., Tesakova, E.M., Kharitonov, V.M., and Shcherbinina, E.A., Upper Cretaceous deposits in the northwest of Saratov oblast, Part 1: Litho- and biostratigraphic analysis of the Vishnevoe section, *Stratigr. Geol. Correl.*, 2007, vol. 15, no. 6, pp. 610–655.

Olfer'ev, A.G., Beniamovsky, V.N., Ivanov, A.V., Ovechkina, M.I., Seltser V.B., and Kharitonov, V.M., Upper Cretaceous of north Saratov Region. 2. Biostratigraphic subdivision of Bolshevik Quarry section in vicinity of Volsk, *Byull. Mosk. O–va Ispyt. Prir., Otd. Geol.*, 2009, vol. 84, no. 4, pp. 29–46.

Ovechkina, M.N., Kopaevich, L.F., Aleksandrova, G.N., Proshina, P.A., Ryabov, I.A., Baraboshkin, E.Yu., Guzhikov, A.Yu., and Mostovski, M.B., Calcareous nannofossils and other proxies define the Santonian–Campanian boundary in the Central Crimean Mountains (Alan-Kyr section), *Cretaceous Res.*, 2021, vol. 119, 104706. https://doi.org/10.1016/j.cretres.2020.104706

Pearce, M.A., Jarvis, I., Ball, P.J., and Laurin, J., Palynology of the Cenomanian to lowermost Campanian (Upper Cretaceous) chalk of the Trunch Borehole (Norfolk, UK) and a new dinoflagellate cyst bioevent stratigraphy for NW Europe, *Rev. Palaeobot. Palynol.*, 2020, vol. 278, 104188. https://doi.org/10.1016/j.revpalbo.2020.104188

Pechersky, D.M. and Safonov, V.A., Palinspastic reconstruction of the position of the Crimean Mountains in Middle Jurassic–Early Cretaceous based on paleomagnetic data, *Geotektonika*, 1993, no. 1, pp. 96–105.

Petters, S.W., Bolivinoides evolution and Upper Cretaceous biostratigraphy of the Atlantic Coastal Plain of New Jersey, *J. Paleontol.*, 1977, vol. 51, pp. 1023–1036.

Pokrovsky, B.G., Bujakaite, M.I., Petrov, O.L., and Kolesnikova, A.A. The C, O, and Sr isotope chemostratigraphy of the Vendian (Ediacaran) - Cambrian transition, Olekma River, western slope of the Aldan Shield, *Stratigr. Geol. Correl.*, 2020, vol. 28, no. 5, pp. 479–492.

Premoli Silva, I. and Sliter, W.V., Cretaceous planktonic foraminiferal biostratigraphy and evolutionary trends from the Botaccione section, Gubbio, Italy, *Palaeontogr. Ital.*, 1995, vol. 82, pp. 1–89.

Premoli Silva, I. and Sliter, W.V., Cretaceous paleoceanography: evidence from planktonic foraminiferal evolution, in *The Evolution of Cretaceous Ocean-Climatic System*, Barrera, E. and Jonson C.C., Eds., *Geol. Soc. Am. Spec. Pap.*, 1999, vol. 332, pp. 301–328.

Prince, I.M., Jarvis, I., and Tocher, B.A., High-resolution dinoflagellate cyst biostratigraphy of the Santonian–basal Campanian (Upper Cretaceous): New data from Whitecliff, Isle of Wight, England, *Rev. Palaeobot. Palynol.*, 1999, vol. 105, pp. 143–169.

Razmjooei, M.J., Thibault, N., Kani, A., Mahanipour, A., Boussaha, M., and Korte, C., Coniacian–Maastrichtian calcareous nannofossil biostratigraphy and carbon-isotope stratigraphy in the Zagros Basin (Iran): Consequences for the correlation of Late Cretaceous stage boundaries between the Tethyan and Boreal realms, *Newsl. Stratigr.*, 2014, vol. 47/2, pp. 183–209.

Razmjooei, M.J., Thibault, N., Kani, A., Dinarès-Turell, J., Pucéat, E., Shahriari, S., Radmacher, W., Jamali, A.M., Ullmann, C.V., Voigt, S., and Cocquerez, T., Integrated bio- and carbon-isotope stratigraphy of the Upper Cretaceous Gurpi Formation (Iran): a new reference for the eastern

Tethys and its implications for large-scale correlation of stage boundaries, *Cretaceous Res.*, 2018, vol. 91, pp. 312–340.

Razmjooei, M.J., Thibault, N., Kani, A., Ullmann, C.V., and Jamali, A.M., Santonian-Maastrichtian carbon-isotope stratigraphy and calcareous nannofossil biostratigraphy of the Zagros Basin: long-range correlation, similarities and differences of carbon-isotope trends at global scale, *Global Planet. Change*, 2020, vol. 184, no. 103075.

Remane, J., Basset, M.G., Cowie, J.W., Gohrbandt, K.H., Lane, H.R., Michelsen, O., and Wang, N., Revised guidelines for the establishment of global chronostratigraphic standards by the International Commission on Stratigraphy (ICS), *Episodes*, 1996, vol. 19, no. 3, pp. 77–81.

Robaszynski, F. and Caron, M., Foraminifères planctoniques du Cretace: Commentaire de la zonation Europe-Mediterranee, *Geol. Soc. Am. Bull.*, 1995, vol. 166, no. 6, pp. 681–692.

Rud'ko, S.V., Kuznetsov, A.B., and Piskunov, V.K., Sr isotope chemostratigraphy of Upper Jurassic carbonate rocks in the Demerdzhi Plateau (Crimean Mountains), *Stratigr. Geol. Correl.*, 2014, vol. 22, no. 5, pp. 494–506.

Rud'ko, S.V., Kuznetsov, A.B., and Pokrovsky, B.G., Sr chemostratigrphy, δ13C, and δ18O of rocks in the Crimean carbonate platform (Late Jurassic, northern Peri-Tethys), *Lithol. Miner. Resour.*, 2017, vol. 52, no. 6, pp. 479–497.

Schulz, M.-G., Ernst, G., Ernst, H., and Schmid, F., Coniacian to Maastrichtian stage boundaries in the standard section for the Upper Cretaceous white chalk of NW Germany (Lägerdorf-Kronsmoor-Hemmoor): Definitions and proposals, *Bull. Geol. Soc. Denmark*, 1984, no. 33, pp. 203–215.

Semikhatov, M.A., Kuznetsov, A.B., Podkovyrov, V.N., Bartli, J., and Davydov, Yu.V., The Yudoma complex of the stratotype area: C-isotope chemo-stratigraphic correlations and a correlation with the Vendian, *Stratigr. Geol. Correl.*, 2004, vol. 12, no. 5, pp. 3–29.

Stratigraphical Atlas of Fossil Foraminifera, 2nd ed., Jenkins, D.G. and Murray, J.W., Eds., British Micropalaeontol. Soc. Ser., Ellis Horwood Ltd. Publisher, 1989. Stratigraphy.org—International Commission on Stratigraphy. https://stratigraphy.org/gssps/#cretaceous

Thibault, N., Jarvis, I., Voigt, S., Gale, A.S., Attree, K., and Jenkyns, H.C., Astronomical calibration and global correlation of the Santonian (Cretaceous) based on the marine carbon isotope record, *Paleoceanography*, 2016, vol. 31, pp. 847–865.

Vandenberg, J., New paleomagnetic data from the Iberian Peninsula, in *Paleomagnetism and the Changing Configuration of the Western Mediterranean Area in the Mesozoic and Early Cenozoic Eras, Geol. Ultraiectina*, 1979, vol. 20, pp. 155–178.

Vandenberg, J. and Wonders, A.A.H., Paleomagnetism of late Mesozoic pelagic limestones from the Southern Alps, *J. Geophys. Res.*, 1980, vol. 85, no. B7, pp. 3623–3627.

Vishnevskaya, V.S. and Kopaevich, L.F., Microfossil assemblages as key to reconstruct sea-level fluctuations, cooling episodes and palaeogeography: The Albian to Maastrichtian of Boreal and Peri-Tethyan Russia, *Spec. Publ.—Geol. Soc. London.*, 2020, vol. 498, pp. 165–187. https://doi.org/10.6084/m9.figshare.c.4737236

Wagreich, M., Summesberger, H., and Kroh, A., Late Santonian bioevents in the Schattau section, Gosau Group of Austria—implications for the Santonian–Campanian boundary stratigraphy, *Cretaceous Res.*, 2010, vol. 31, pp. 181–191.

Walaszczyk, I. and Peryt, D., Inoceramid-foraminiferal biostratigraphy of the Turonian through Santonian deposits of the Middle Vistula Section, Central Poland, *Zbl. Geol. Palaönt.*, 1998, vol. I, nos. 11/12, pp. 1501–1503.

Walaszczyk, I., Dubicka, Z., Olszewska-Nejbert, D., and Remin, Z., Integrated biostratigraphy of the Santonian through Maastrichtian (Upper Cretaceous) of extra-Carpathian Poland, *Acta Geol. Polon.*, 2016, vol. 66, pp. 313–350.

Wendler, I., A critical evaluation of carbon isotope stratigraphy and biostratigraphic implications for Late Cretaceous global correlation, *Earth-Sci. Rev.*, 2013, vol. 126, pp. 116–146.

Wierzbowski, H., Anczkiewicz, R., Pawlak, J., Rogov, M.A., and Kuznetsov, A.B., Revised Middle–Upper Jurassic strontium isotope stratigraphy, *Chem. Geol.*, 2017, vol. 466, pp. 239–255.

Williams, G.L., Ascoli, P., Barss, M.S., Bujak, J.P., Davies, E.H., Fensome, R.A., and Williamson, M.A., Chapter 3. Biostratigraphy and related studies, in *Geology of the Continental Margin of Eastern Canada*, Keen, M.J. and Williams, G.L., Eds., *Geol. Surv. Can.*, 1990, vol. 2, pp. 87–137.

Williams, G.L., Brinkhuis, H., Pearce, M.A., Fensome, R.A., and Weegink, J.W., Southern Ocean and global dinoflagellate cyst events compared: Index events for the Late Cretaceous–Neogene, in *Proc. Ocean Drill. Program. Sci. Res.*, Exon, N.F., Kennett, J.P., and Malone, M.J., Eds., 2004, vol. 189, pp. 1–98.

Wolfgring, E., Wagreich, M., Dinarés-Turell, J., Gier, S., Böhm, K., Sames, B., and Spötl, K., The Santonian–Campanian boundary and the end of the Long Cretaceous Normal Polarity-Chron: isotope and plankton stratigraphy of a pelagic reference section in NW Tethys (Austria), *Newsl. Stratigr.*, 2018a. https://www.researchgate.net/publication/325022888.

Wolfgring, E., Wagreich, M., Dinarés-Turell, J., Yilmaz, I.O., and Böhm, K., Plankton biostratigraphy and magnetostratigraphy of the Santonian–Campanian boundary interval in the Mudurnu–Göynük Basin, northwestern Turkey, *Cretaceous Res.*, 2018b, vol. 87, pp. 296–311.

Zubov, A.G. and Kir'yanov, V.Yu., On the possibility of using thermomagnetic parameters for identification of volcanic ashes, in *Geodinamika i vulkanizm Kurilo-Kamchatskoi ostrovoduzhnoi sistemy* (Geodynamics and Volcanism of the Kuril–Kamchatka Island-Arc System), Ivanov, B.V., Ed., Petropavlovsk-Kamchatsky: GEOS, 2001, pp. 267–273.

Zakharov, Y.D., Baraboshkin, E.Y., Weissert, H., Michailova, I.A., Smyshyaeva, O.P., and Safronov, P.P., Late Barremian–early Aptian climate of the northern middle latitudes: stable isotope evidence from bivalve and cephalopod mollusks of the Russian Platform, *Cretaceous Res.*, 2013, vol. 44, pp. 183–201.

Translated by I. Melekestseva